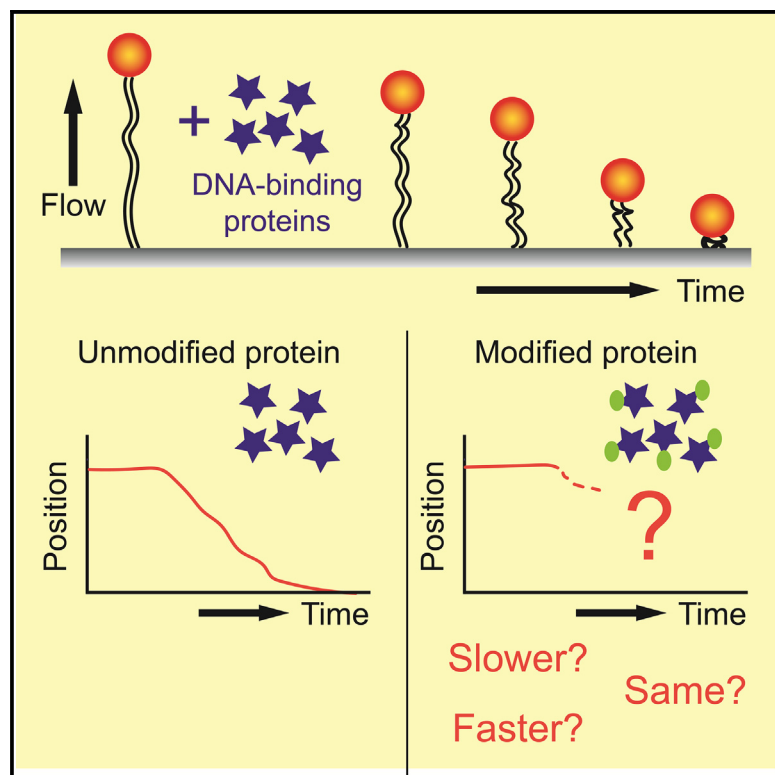


A framework to validate fluorescently labeled DNA-binding proteins for single-molecule experiments

Graphical abstract



Authors

Miranda Molina, Lindsey E. Way,
Zhongqing Ren, ..., Brandon Shields,
Xindan Wang, HyeongJun Kim

Correspondence

xindan@indiana.edu (X.W.),
hyeongjun.kim@utrgv.edu (H.K.)

In brief

Introducing a short peptide such as lysine-cysteine-lysine (KCK) tag is one of the commonly used fluorescent-dye labeling strategies. Molina et al. show that single-molecule DNA flow-stretching assay is a versatile tool to detect unwanted protein property changes. Their results highlight that rigorous validations are required when studying modified proteins.

Highlights

- KCK tag can alter protein properties both quantitatively and qualitatively
- Electrostatic interactions between the KCK tag and DNA contribute to the artifacts
- Adding a short peptide tag to ParB protein does not lead to its *in vivo* changes
- Single-molecule DNA flow-stretching assay can detect protein property changes

Resource

A framework to validate fluorescently labeled DNA-binding proteins for single-molecule experiments

Miranda Molina,^{1,2,4,5} Lindsey E. Way,^{3,5} Zhongqing Ren,³ Qin Liao,³ Bianca Guerra,² Brandon Shields,² Xindan Wang,^{3,*} and HyeongJun Kim^{1,2,6,*}

¹Biochemistry and Molecular Biology Program, University of Texas Rio Grande Valley, Edinburg, TX 78539, USA

²Department of Physics and Astronomy, University of Texas Rio Grande Valley, Edinburg, TX 78539, USA

³Department of Biology, Indiana University, 1001 E 3rd St., Bloomington, IN 47405, USA

⁴Present address: Long School of Medicine, UT Health Science Center at San Antonio, San Antonio, TX 78229, USA

⁵These authors contributed equally

⁶Lead contact

*Correspondence: xindan@indiana.edu (X.W.), hyeongjun.kim@utrgv.edu (H.K.)

<https://doi.org/10.1016/j.crmeth.2023.100614>

MOTIVATION Single-molecule fluorescence microscopy has been extensively used in modern biology to define the molecular action of proteins. Appending short peptide tags is a common strategy to enhance fluorescence labeling. Here, we evaluate the impact of a commonly used tag, the lysine-cysteine-lysine (KCK) tag, on protein behavior in single-molecule DNA flow-stretching assay, which is a sensitive and versatile method to understand the action of DNA-binding proteins. Our motivation is to provide researchers with an experimental framework to validate fluorescently labeled DNA-binding proteins in single-molecule methods.

SUMMARY

Due to the enhanced labeling capability of maleimide-based fluorescent probes, lysine-cysteine-lysine (KCK) tags are frequently added to proteins for visualization. In this study, we employed an *in vitro* single-molecule DNA flow-stretching assay as a sensitive way to assess the impact of the KCK tag on the property of DNA-binding proteins. Using *Bacillus subtilis* ParB as an example, we show that, although no noticeable changes were detected by *in vivo* fluorescence imaging and chromatin immunoprecipitation (ChIP) assays, the KCK tag substantially altered ParB's DNA compaction rates and its response to nucleotide binding and to the presence of the specific sequence (*parS*) on the DNA. While it is typically assumed that short peptide tags minimally perturb protein function, our results urge researchers to carefully validate the use of tags for protein labeling. Our comprehensive analysis can be expanded and used as a guide to assess the impacts of other tags on DNA-binding proteins in single-molecule assays.

INTRODUCTION

Fluorescence-based protein visualization has played an instrumental role in single-molecule experiments.^{1–5} Intensive research has led to fruitful development of a variety of fluorophores and tagging methods for proteins.^{6–10} Regardless of the kinds of probes and labeling modalities, the main goals have remained largely unchanged: achieving adequate fluorescence labeling while minimally perturbing the properties of the proteins.

Unwanted alteration of protein properties can occur at any stage during the preparation of the labeled protein, which must be minimized to reveal the true function of the protein of interest.

First, introducing additional components into a protein requires careful consideration during the protein design. The sizes of common fluorescent proteins are around 25 kD,^{5,11} and those of self-labeling proteins SNAP, CLIP, and Halo tags are about 20, 20, and 33 kDa, respectively.¹² It has been well appreciated that large protein tags could interfere with the protein's function and disrupt protein-protein interactions, and smaller tags are preferred.^{3,13} Second, fluorescent-dye labeling steps can adversely affect protein activities. For example, *Bacillus subtilis* structural maintenance of chromosomes (BsSMC) protein is capable of compacting flow-stretched DNA.¹⁴ We previously observed that using a centrifugal concentrator-based method to remove unreacted fluorescent dyes abolished BsSMC's

DNA compaction ability, whereas using a resin-based column did not.¹⁴ Third, fluorescent dyes could disrupt the proper functioning of a protein itself. Especially, it has been shown that hydrophobic fluorescent dyes have a potential to cause artifacts due to nonspecific binding.¹⁵ Lastly, fluorescently labeled proteins may malfunction in the context of experimental environments. Prominent examples were reported with quantum dot (QD)-labeled proteins. Effective diameters of commercially available functionalized QDs (“big” QDs) are in the 14–35 nm range,¹⁶ while “small” QDs are 9–12 nm in diameter.^{17,18} When the localizations of AMPA receptors (AMPAR) on neurons were examined, big QD-labeled AMPARs localized differently from small QD-labeled (or 4-nm organic fluorescent-dye-labeled) AMPARs, along with difference in diffusion coefficients, possibly due to the narrow synaptic cleft size (~30 nm).^{19,20}

While fluorescently tagged proteins are crucial in a variety of biological studies, a challenge is the lack of predictions for how the fluorescent tags or probes will alter protein function. Thus, empirical investigations must follow. The purpose of this study is to explore the single-molecule DNA flow-stretching assay as a sensitive and efficient tool to test whether a tag alters the function of a DNA-binding protein. We chose the DNA flow-stretching approach because it has been extensively used in studying actions of DNA-binding proteins on individual DNA molecules.^{14,21–26} Furthermore, contrary to force-based single-molecule assays that visualize one DNA molecule at a time, single-molecule DNA flow-stretching assay allows 10–40 DNA molecules to be analyzed in each field of view, which is advantageous for subsequent statistical data analyses.

In this study, for a proof of principle, we tested the effect of lysine-cysteine-lysine (KCK) tag on *B. subtilis* ParB (BsParB) proteins. We chose this tag because maleimide-conjugated fluorescent dyes have been widely used to label proteins via covalent conjugation to surface-exposed cysteines.¹ However, labeling all desired cysteines with maleimide dyes is not always achieved. The reaction efficiency between the thiol group on cysteine and the maleimide moiety of a fluorescent dye can be increased by flanking the cysteine with two positively charged lysine residues. It was revealed that the neighboring lysine residues decrease pKa of the cysteine residue, thereby increasing thiol-maleimide reactivity.^{27–30} Thus, appending the KCK tag to a protein has been a popular and extensively used method due to its superior fluorescence-labeling efficiency.^{23,31–37}

We chose ParB protein as our example because of its well-known *in vivo* and *in vitro* activities. The ParABS DNA partitioning system is a broadly conserved segregation machinery for bacterial chromosomes and plasmids. ParB binds to *parS* sequences and spreads to neighboring regions^{38,39} to form a nucleoprotein complex, which is translocated by ParA.^{38,39} *In vivo*, ParB spreading is evident by two approaches: fluorescence microscopy in which fluorescently tagged ParB proteins form foci in live cells and chromatin immunoprecipitation (ChIP) assays in which ParB protein associates with 10–20 kb DNA regions encompassing *parS*.^{38,39} Importantly, it was recently discovered that ParB protein is a novel enzyme that utilizes cytidine triphosphate (CTP) to modulate ParB spreading.^{40–42} *In vitro*, ParB’s spreading has been shown by imaging fluorescently labeled

ParB proteins on doubly tethered (or doubly trapped) DNAs with protein load blocks.^{41,43,44} In addition, previous single-molecule DNA flow-stretching assays have reported that ParB’s DNA compaction activity *in vitro* is correlated with ParB’s spreading activity *in vivo*.²³ Here we report that DNA compaction by ParB is artificially enhanced by KCK tags in single-molecule DNA flow-stretching assays *in vitro*. Further investigation indicates that electrostatic interactions between the negatively charged DNA backbone and the positively charged KCK tag contribute at least partly to these artifacts that are not rescued even with fluorophore labeling onto the KCK tag. Contrary to the *in vitro* single-molecule results, the KCK tag did not lead to any noticeable changes *in vivo*. In sum, our single-molecule DNA flow-stretching assay is highly sensitive and allows the detection of the property changes in DNA-binding proteins for single-molecule experiments. Its high-throughput data production allows statistical analyses and leads to conclusions more efficiently. We propose that the DNA flow-stretching-based approaches can be used as a tool to detect property changes of DNA-binding proteins upon addition of tags or fluorescent probes.

RESULTS

KCK tags increase BsParB’s DNA compaction rates *in vitro*

KCK tags are frequently used for *in vivo* and *in vitro* protein labeling due to their small size and the increased labeling efficiency of maleimide-fluorescence dyes.^{27–30} To understand whether this three-amino-acid tag has any impact on ParB proteins, we purified tagged and untagged wild-type *B. subtilis* ParB (BsParB(WT)) proteins (Figure S1A) and employed single-molecule DNA flow-stretching assays with a lambda DNA substrate (Figure 1A). Since ParB has been shown to be a CTPase,^{40–42} our samples were treated with apyrase to remove residual nucleotides from our protein samples. Upon addition of the purified proteins, we measured the speed of DNA compaction by tracking the positions of a fluorescent QD labeled at one DNA end (Figure 1B).²³ In the presence of 50 nM untagged BsParB(WT), we observed robust DNA compaction all the way to the DNA tether point in the absence of CTP as previously shown (Figures 1B and S2).²³ Interestingly, both 1 mM CTP and CTP γ S (a non-hydrolyzable CTP analog) dramatically inhibited DNA compaction rates, by 39-fold and 149-fold, respectively (Figures 1C and S1D, three blue bars, and Figure S3A), implying counter-productive roles of CTP binding in DNA compaction. The mechanism of CTP binding on ParB’s action is currently being investigated in a separate study. When BsParB(WT) with the KCK tag at its N terminus (hereafter “KCK-BsParB(WT)”) (Figure S1A) was subjected to the same experiment, without CTP, we observed that the lambda DNA was compacted to the tether point at a slightly slower rate (at 0.72x) than BsParB(WT) (Figures 1C and S1D, compare the first blue and red bars, and Figure S2). Conversely, in the presence of CTP or CTP γ S, KCK-BsParB(WT) exhibited much higher DNA compaction rates than BsParB(WT), at 10.5-fold for CTP (Figures 1C and S1D, compare second blue and red bars) and 19.4-fold for CTP γ S (Figures 1C and S1D, compare third blue

Cell Reports Methods

Resource

CellPress
OPEN ACCESS

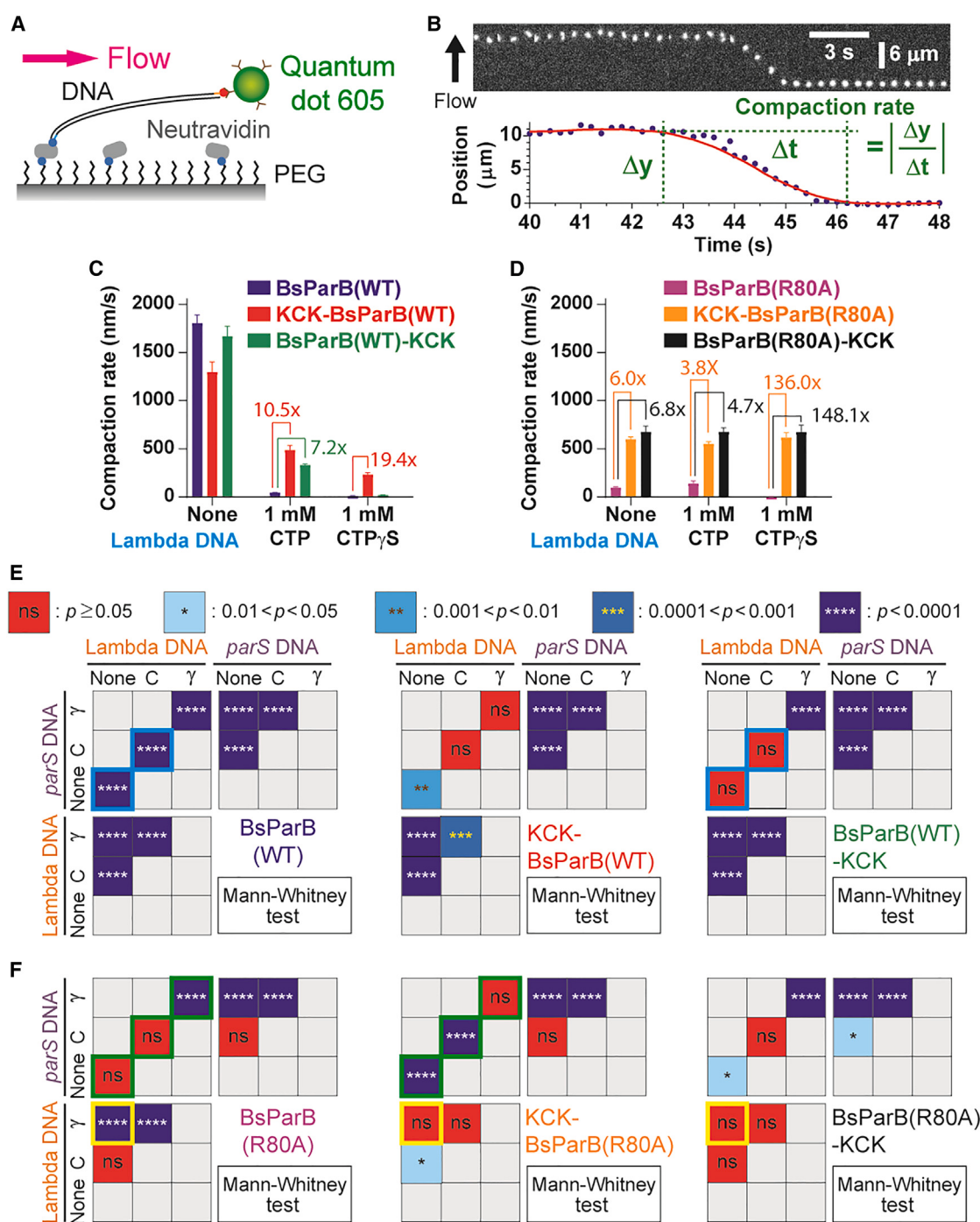


Figure 1. In vitro quantitative and qualitative BsParB compaction rate changes by the KCK tags

(A) Schematic of single-molecule DNA flow-stretching assays.

(B) An example of DNA compaction by 50 nM BsParB(WT) protein (top) and the definition of compaction rate (bottom).

(C and D) Lambda DNA compaction rates by 50 nM (C) wild-type ($n = 30\text{--}74$ from three to eight experiments) and (D) R80A mutant ($n = 29\text{--}58$ from three to four experiments) proteins. Numbers indicate compaction rate fold increases. Error bars: SEM.

(E) Top: Mann-Whitney test (the Wilcoxon rank-sum test) p value color scheme. Bottom: Mann-Whitney test comparisons for compaction rates by wild-type BsParB and its KCK versions.

(F) Mann-Whitney test comparisons for BsParB(R80A) and its KCK versions. (E and F) Cyan, green, and yellow boxes highlight qualitative protein property changes due to the KCK tags for visual aids. (C-F) See Tab 1 in Data S1 for detailed sample number (n) information. See also Figures S1–S3, S5, and S7.

and red bars). As seen in **Figures 1C** and **S1D** (compare the three red bars), adding the nucleotides only reduced KCK-BsParB(WT)'s DNA compaction rate by 2.7-fold for CTP and 2.5-fold for CTP γ S, whereas, mentioned earlier, BsParB(WT)'s response to nucleotides was much more dramatic (**Figures 1C** and **S1D**, three blue bars) (also see **Figure S3A**).

We note that although the purified proteins were stored in a buffer that contains 5 mM β -mercaptoethanol, which is a reducing agent that blocks disulfide bridge formations between cysteines, the imaging experiments were conducted in buffers without reducing agents. To understand whether reducing agents could make a difference, we added 1 mM β -mercaptoethanol (**Figure S3B**) or 1 mM dithiothreitol (DTT) (**Figure S3C**) to our imaging experiments. We observed that these reducing agents resulted in nonspecific binding of QD-DNA-protein onto the sample chamber surface or the decrease of fluorescence intensity of the QD (**Figures S3B** and **S3C**). Nevertheless, in the presence of DTT, supplementing CTP still caused 2.8-fold DNA compaction rate decrease using KCK-BsParB(WT) (**Figure S3D**), which was the same trend observed without reducing agents (**Figures 1C** and **S3A**). Thus, the reducing agents did not alter our experimental conclusions. Due to the technical challenges of our imaging experiments in the presence of reducing agents (**Figures S3B** and **S3C**), we have performed further experiments without them.

Of note, in our experience, batch-to-batch variations in purified proteins only lead to up to 2-fold differences for DNA compaction rates. The dramatic changes in protein behavior caused by KCK tags (**Figures 1C** and **S1D**) prompted us to investigate further.

Next, we examined the effect of ParB-specific *parS* sequence on DNA compaction rates by inserting a *parS* in the middle of the lambda DNA (hereafter, “*parS* DNA”).²³ We found that without any nucleotides, untagged BsParB(WT) compacted *parS* DNA 25% slower than it did for lambda DNA without *parS* (**Figures S1B** and **S1D**). In the presence of CTP or CTP γ S, untagged BsParB(WT)'s compaction rate of *parS* DNA decreased by 16-fold and 50-fold, respectively (**Figures S1B** and **S1D**, three blue bars with lined fill pattern). The mechanism of *parS* on ParB's action is currently being investigated in a separate study. Strikingly, KCK-BsParB(WT) exhibited substantial increase in the *parS* DNA compaction rates in the presence of CTP (4.9-fold, compare second blue and red bars with lined fill pattern) or CTP γ S (7.2-fold, compare third blue and red bars with lined fill pattern) compared with untagged BsParB(WT) (**Figures S1B** and **S1D**). Thus, the KCK tag enhanced BsParB(WT)'s DNA compaction rate (compared to the untagged BsParB(WT)) when nucleotides are present on both lambda DNA and *parS* DNA.

Given that ParB protein's CTP binding pocket resides at the N-terminal domain (NTD) and the NTD is implicated to be the DNA entry gate,^{41,42,45} we questioned if the unexpected compaction rate increases also occur when KCK is tagged at the C terminus of BsParB(WT) protein (hereafter, “BsParB(WT)-KCK”) (**Figure S1A**). Indeed, like KCK-BsParB(WT), BsParB(WT)-KCK also showed much faster compaction with CTP compared with BsParB(WT) (**Figure 1C** for the lambda DNA; **Figure S1B** for the *parS* DNA). Thus, KCK enhanced

BsParB(WT)'s DNA compaction rate when appended to either terminus.

KCK tags alter BsParB's DNA compaction properties in response to nucleotides and *parS*

To quantify how the BsParB(WT) protein and its KCK-tagged variants respond to different nucleotides and a *parS* site, Mann-Whitney tests were performed for DNA compaction rates with all possible permutations (**Figure 1E**; also see **Figure S1E**). Our analyses revealed that, without any nucleotide or with CTP, BsParB(WT) was responsive to the existence of *parS* ($p < 0.001$), while BsParB(WT)-KCK did not make statistically significant compaction rate changes with *parS* ($p \geq 0.05$) (see cyan boxes in **Figure 1E**). We note that the KCK tags not only changed compaction rates (**Figures 1C**, **S1B**, and **S1D**) but also reversed the trend of compaction. Specifically, without nucleotides, when a *parS* site was added to DNA, BsParB(WT)'s compaction rate was slowed down, but KCK-BsParB(WT)'s compaction rate was increased (**Figure S1D**). These results show that the KCK tag alters the DNA compaction ability both quantitatively and qualitatively.

The KCK tag alters the action of BsParB R80A mutant

We next investigated whether the compaction rate change induced by the KCK tag was limited only to the wild-type BsParB. The R80A mutant of BsParB has been shown to abolish proper *in vivo* sporulation, localization, and spreading along with *in vitro* lambda DNA compaction in the absence of nucleotides.^{23,46,47} Surprisingly, without nucleotides, although its DNA compaction rate was 18.2-fold lower than BsParB(WT) (**Figure S1D**, compare first blue and purple bars), BsParB(R80A) (**Figure S1A**) was still capable of compacting the lambda DNA (**Figure 1D**), contradicting a previous report (see *discussion*).²³ Next, we wondered whether a KCK tag alters BsParB(R80A)'s action on DNA. Indeed, with lambda DNA, the compaction rates of both KCK-BsParB(R80A) and BsParB(R80A)-KCK were substantially increased for all tested nucleotides (**Figures 1D** and **S1D**). When *parS* DNA was used as a substrate, compaction rate increases by KCK tags ($p < 0.0001$) were also noted (**Figures S1C** and **S1D**). The visualized Mann-Whitney comparison charts for DNA compaction rates highlight that BsParB(R80A), KCK-BsParB(R80A), and BsParB(R80A)-KCK respond differently to different nucleotides and the presence of *parS* (see green and yellow boxes in **Figure 1F**; also see **Figure S1F**).

The effects of KCK tags on protein action are limited to *in vitro* assays but not *in vivo*

The different effects of KCK tags on DNA compaction *in vitro* prompted us to systematically test the effect of KCK tag on BsParB's or BsParB(R80A)'s localization and spreading *in vivo*. We first generated eight GFP fusions to the ParB variants with KCK tags at the C or N terminus of the protein and performed fluorescence microscopy (**Figure 2A**). Consistent with previous findings that R80A abolishes ParB spreading,²³ BsParB(WT) formed foci in the cells, while BsParB(R80A) had diffused localization on the DNA. Interestingly, KCK tags at the C or N terminus did not alter the localization of ParB(WT) or ParB(R80A) (**Figure 2A**). In a complementary approach, we analyzed the *in vivo*

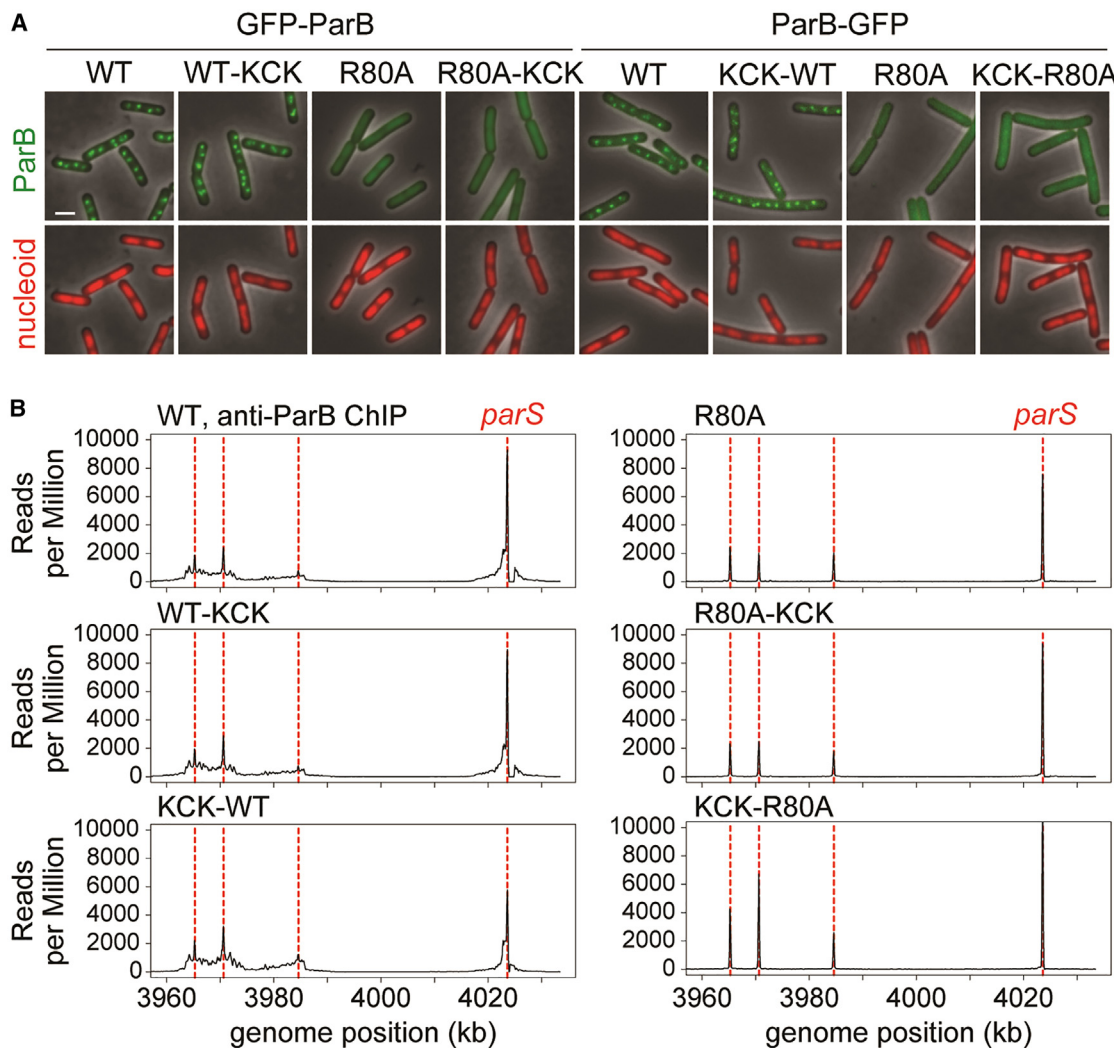


Figure 2. KCK tags do not affect *in vivo* BsParB localization or spreading

(A) Localization of fluorescently tagged ParB(WT) and ParB(R80A) (green). The nucleoid is labeled with HBSU-mCherry (red), and phase-contrast images are shown in gray. Scale bar represents 2 μ m. The imaging experiments were performed in two biological replicates, and representative images from one set of experiment are shown.

(B) ChIP-seq of wild-type and mutant ParB association with a region of the *B. subtilis* chromosome from 354° to 360° (3,960- to 4,033-kb of strain the PY79 genome). Red dotted lines indicate the positions of the four *parS* sites. The number of reads were normalized by the total number of reads per sample. Whereas wild-type ParB spreads several kilobases from *parS* sites, the R80A mutant is restricted to the immediate vicinity of each *parS* site. KCK tags at the N terminus or C terminus of wild-type ParB or R80A mutant do not change the property of the variants. One ChIP-seq replicate was done. See also Figure S4.

spreading of ParB variants on the genome by chromatin immunoprecipitation (ChIP-seq) assays using anti-ParB antibodies (Figure 2B). We observed that BsParB(WT) spreads to an ~20-kb region surrounding the *parS* site, but BsParB(R80A) did not spread. These results are consistent with previously published data.²³ Importantly, having a KCK tag at the C or N terminus did not affect the spreading of BsParB(WT) or BsParB(R80A). We also show that the KCK-tagged proteins have similar expression levels compared to the matched untagged controls (Figures S4A and S4B). These experiments demonstrate that the KCK tag does not affect BsParB's functions *in vivo*. Thus, the effects of KCK tags on BsParB(WT) and BsParB(R80A) are specific to *in vitro* experiments.

Charges on the KCK tag contribute to the *in vitro* protein property changes

This finding prompted us to understand the mechanism by which the KCK tag boosts the DNA compaction rate of ParB protein *in vitro*. One possibility for the compaction rate increase is that more BsParB proteins were recruited onto DNA due to interactions between the positively charged KCK tag and the negatively charged DNA backbone. Alternatively, the KCK tag could impact the subsequent action of the BsParB proteins, while the level of the initial protein recruitment is intact. To distinguish these two possibilities, we directly visualized the recruitment of untagged and KCK-tagged BsParB(R80A) proteins onto lambda DNA. Proteins were nonspecifically labeled with the NHS ester version of

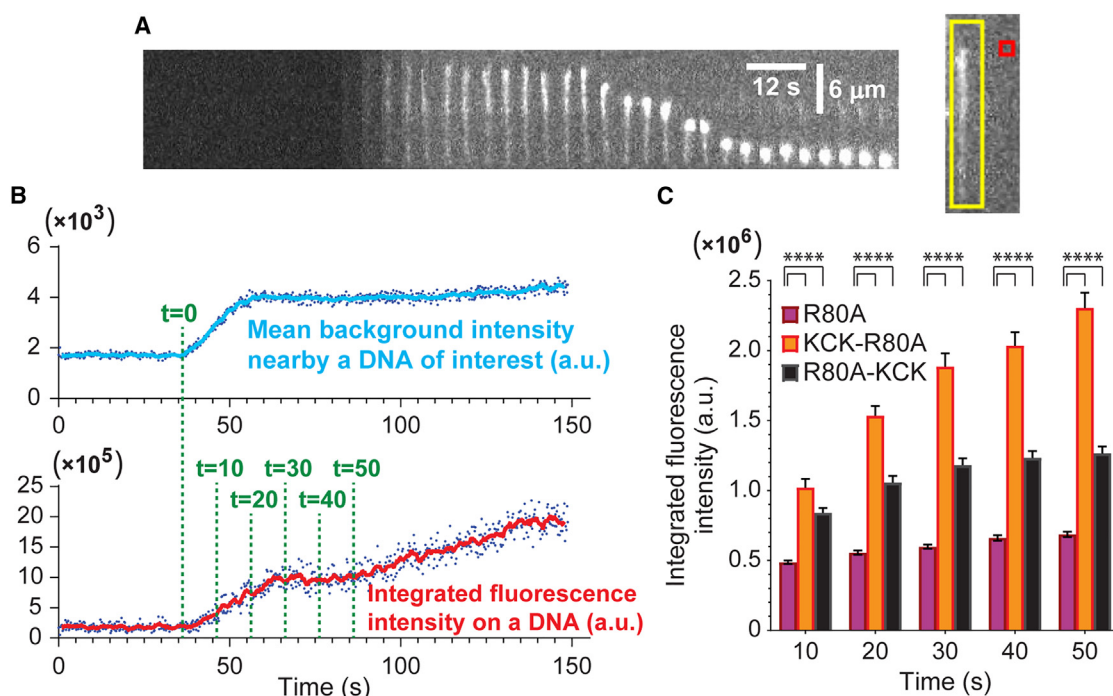


Figure 3. More BsParB(R80A) proteins are loaded onto flow-stretched lambda DNAs when the KCK tag is appended

(A) (Left) A representative kymograph for DNA flow-stretching experiments with fluorescently labeled BsParB protein. 30 nM KCK-BsParB(R80A) without any nucleotides. (Right) The mean background intensity was obtained for the area bound by the red square ($0.96 \times 0.96 \mu\text{m}$), and the background-subtracted integrated fluorescence intensity was obtained for the area bound by the yellow box ($2.4 \times 14.4 \mu\text{m}$).

(B) Time trajectories for mean background and integrated fluorescence intensities on the DNA shown in (A). The time point when the mean background intensity starts to increase is defined as t = 0. DNA flow-stretching experiments were performed with fluorescently labeled proteins.

(C) Integrated fluorescence intensities on lambda DNAs by cyanine3-labeled BsParB(R80A) (n = 51 from two experiments), KCK-BsParB(R80A) (n = 40 from two experiments), and BsParB(R80A)-KCK (n = 26 from three experiments) measured at different time points. Error bars: SEM; ****p < 0.0001. See also Figure S5.

cyanine3 fluorescent dye, and the moment of the very first labeled protein's arrival into the camera's field of view was evident by increase in background intensity (Figures 3A and 3B). In this approach, background-subtracted integrated fluorescence intensity on DNA is directly proportional to the amount of BsParB protein recruited onto the DNA. The microscopy showed that the background-subtracted integrated fluorescence intensities with KCK-BsParB(R80A) and BsParB(R80A)-KCK in the absence of CTP were higher than those with BsParB(R80A) ($p < 0.0001$) (Figure 3C, compare it with Figure 1D). A similar trend was observed using BsParB(WT), KCK-BsParB(WT), and BsParB(WT)-KCK (Figures S5A and S5B). Thus, our data show that DNA compaction rates by BsParB protein variants are correlated with the degree of protein loading onto DNA, although our experimental approaches do not address if the KCK tags impact subsequent protein action after being recruited onto DNA.

To address whether the charge of KCK tags was the issue, we prepared recombinant wild-type and R80A mutant BsParB proteins where a negatively charged glutamic acid-cysteine-glutamic acid (ECE) tag was added to the N terminus of proteins. If electrostatic interactions between the appended tags and DNA backbone contribute to *in vitro* artifacts, slower compaction rates are expected with ECE-tagged BsParB proteins (hereafter "ECE-BsParB") due to repulsive forces be-

tween negative charges. As expected, DNA compactions by ECE-BsParB(R80A) were noticeably inefficient. The compaction rates by ECE-BsParB(R80A) are significantly lower ($0.001 < p < 0.01$ and $p < 0.0001$) than those by BsParB(R80A) regardless of the presence of the *parS* DNA sequence and CTP (Figure 4A). Consistent with this observation, the ECE-BsParB(WT) protein also exhibits inefficient DNA compaction compared with its BsParB(WT) counterpart in the absence of any nucleotides (Figure S6).

Next, we investigated any *in vivo* property changes caused by the N-terminally appended ECE tag. Fluorescence microscopy experiments show that the ECE tag neither abolishes the *in vivo* fluorescence foci formation with the wild-type BsParB protein nor leads to the formation of clear foci with the R80A mutant BsParB (Figure 4B). For instance, clear foci formation was observed with BsParB(WT), KCK-tagged BsParB(WT), and ECE-tagged BsParB(WT) *in vivo*, while the localization of BsParB(R80A), KCK-tagged BsParB(R80A), and ECE-tagged BsParB(R80A) appeared as a haze of green fluorescence in the cytoplasm. Additionally, ChIP-seq assays using anti-ParB antibodies indicate that wild-type BsParB proteins spread to ~20-kb regions around the *parS* site, and the R80A mutant does not spread regardless of the presence of the ECE tag (Figure 4C). All *in vivo* results consistently demonstrate that the KCK and ECE tags appended to BsParB proteins do not have

Cell Reports Methods

Resource

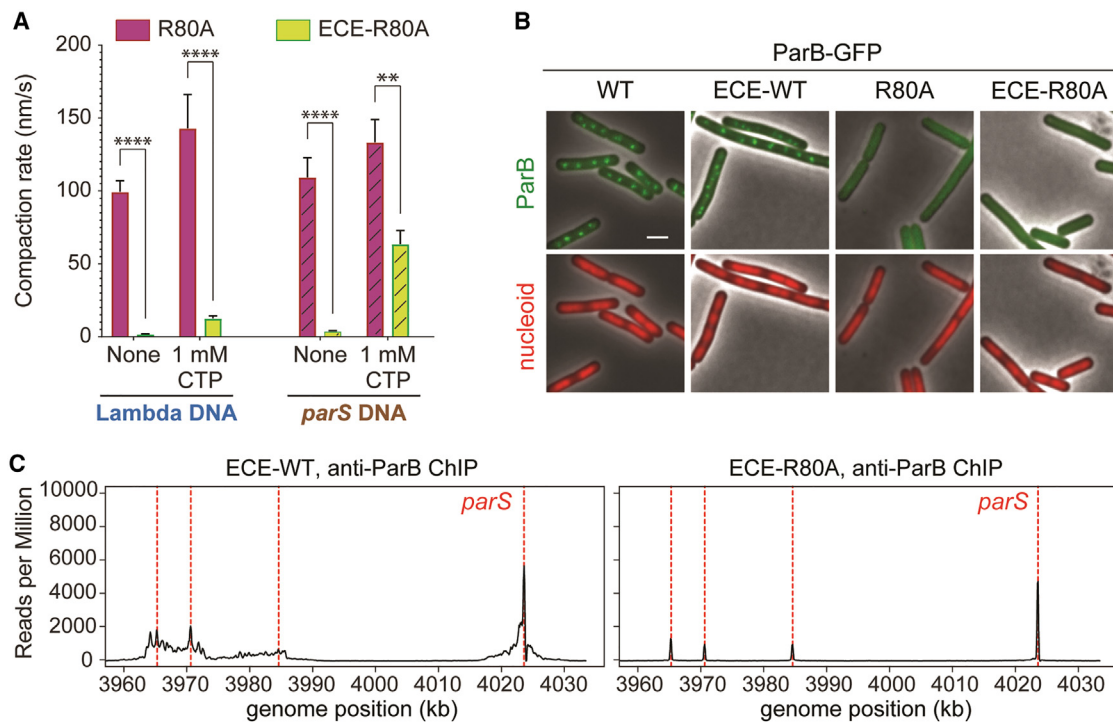


Figure 4. Adding negatively charged ECE tag on BsParB protein slows down DNA compaction *in vitro* but does not lead to *in vivo* changes

(A) Lambda and *parS* DNA compaction rates by BsParB(R80A) ($n = 38\text{--}58$ from three to four experiments) and ECE-BsParB(R80A) ($n = 25\text{--}64$ from three to six experiments) both in the presence and absence of CTP. Error bars: ** $0.001 < p < 0.01$ and **** $p < 0.0001$. See Tab 1 in Data S1 for detailed sample number (n) information.

(B) Localization of fluorescently tagged BsParB(WT), BsParB(R80A), and their ECE-tagged versions (green). Red: the nucleoid labeled with HBsu-mCherry. Gray: phase-contrast images. Scale bar represents 2 μm . The imaging experiment was performed in two biological replicates, and representative images from one set of experiment are shown.

(C) ChIP-seq of ECE-tagged wild-type (left) and mutant ParB (right) association with a region of the *B. subtilis* chromosome from 354° to 360° (3,960- to 4,033-kb of strain the PY79 genome). Red dotted lines indicate the positions of the four *parS* sites. The number of reads were normalized by the total number of reads per sample. Whereas ECE-ParB(WT) spreads several kilobases from *parS* sites, the ECE-R80A mutant is restricted to the immediate vicinity of each *parS* site. One ChIP-seq replicate was done. See also Figure S6.

noticeable impacts. The effects of the tags are only limited to *in vitro* assays, and electrostatic interactions between charged residues on the tag and the DNA backbone are at least partly responsible for the *in vitro* effects.

KCK-tagged BsParB proteins labeled with fluorescent dyes do not behave the same as the untagged protein

In single-molecule experiments, the KCK tag is frequently included in proteins to facilitate maleimide-based labeling. As discussed above, we observed that appending a KCK tag itself caused unexpected *in vitro* behavior changes to BsParB proteins. We next set out to test whether a fluorescent labeling to the KCK tag could reverse the changes and make the KCK-tagged protein behave the same as the untagged protein. We chose Alexa Fluor 647 maleimide as a fluorescent probe because its negative charge may neutralize the effects of positively charged KCK tag. The fluorescence signals from the QD labeled at the end of DNA and Alexa 647-labeled KCK-BsParB(WT) were separated from each other by OptoSplit II image splitter (Cairn Research) and imaged onto different fields of view on the detector. The DNA compaction rates were obtained

by tracking the QD positions in real time. Figures 1C and S3A indicate that CTP addition leads to a dramatic (39-fold) and a moderate (2.7-fold) DNA compaction rate reduction for unlabeled BsParB(WT) and KCK-BsParB(WT), respectively. We used the DNA compaction rate changes between having and not having CTP as a determinant to assess if Alexa 647 maleimide-labeled KCK-BsParB(WT) can behave the same as untagged BsParB(WT). In the presence of CTP, substantial decreases of DNA compaction rate by Alexa 647-KCK-BsParB(WT) were not observed. Qualitatively, the Alexa 647-labeled KCK-BsParB(WT) protein still did not behave like unlabeled BsParB(WT). One technical challenge with this experiment was that at least 30% of QD-DNA-dye-protein nonspecifically bound to the sample chamber surface during the compaction and prevented us from accurate quantification. To further passivate the surface, we flowed in casein and bovine serum albumin (BSA) after tethering DNAs, which was a common strategy used in single-molecule imaging.^{48,49} Then the protein in the imaging buffer (without casein and BSA) was flowed in for single-molecule DNA flow-stretching experiments. This was done not only for Alexa 647-KCK-BsParB(WT) but also for

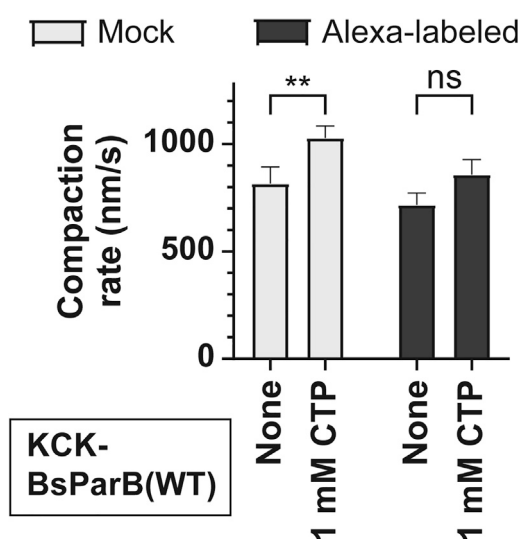


Figure 5. Labeling the cysteine on KCK-BsParB(WT) with Alexa Fluor 647 maleimide does not lead to a significant DNA compaction rate decrease in the presence of CTP

DNA compaction rates by unlabeled KCK-BsParB(WT) from the mock reaction and Alexa 647 maleimide-labeled KCK-BsParB(WT) with lambda DNA ($n = 19\text{--}41$ from three to four experiments). Error bars: SEM; ** $0.001 < p < 0.01$ and ns, not significant ($p > 0.05$).

unlabeled KCK-BsParB(WT) after a mock labeling reaction. Under this experimental condition, the DNA compaction rate by unlabeled KCK-BsParB(WT) in the presence of CTP was 1.3-fold higher than that without CTP (Figure 5) likely due to casein/BSA-treated flow cell surface. The DNA compaction rates by Alexa 647-KCK-BsParB(WT) both in the presence and absence of CTP were comparable to each other, and addition of CTP did not lead to a significant compaction rate decrease (Figure 5) as observed for untagged BsParB(WT) (Figures 1C and S3A). Thus, labeling KCK-BsParB(WT) with a fluorescent probe did not recover the protein properties of untagged BsParB(WT).

DISCUSSION

In this study, we employed a single-molecule DNA flow-stretching assay to measure DNA compaction rates. Contrary to traditional ensemble measurements, single-molecule approaches can reveal unprecedentedly detailed information by looking into individual molecules and providing statistical analyses. Using BsParB protein as an example, we were able to detect the effect of small tags on protein action at high sensitivity across a wide range of conditions.

Fluorescent labeling of BsParB proteins had been mainly achieved by either replacing an amino acid residue with cysteine (such as S68C^{43,50} and L5C⁴⁴) or appending the KCK tag.²³ The previous study showed that KCK-tagged BsParB protein did not lead to disruption on *in vivo* GFP-BsParB foci formation and BsParB-dependent SMC complex (SMC-ScpA-ScpB) localizations.²³ Furthermore, DNA motion capture assay showed that Cy3-labeling of BsParB through the KCK tag did not alter end-biased lambda DNA compaction patterns using *in vitro* assays.²³

However, our thorough assessments of untagged and the KCK-tagged BsParB proteins by the single-molecule DNA flow-stretching assay revealed unexpected alterations in the protein recruitment level and DNA compaction rates.

The increased compaction rates shown with the KCK-tagged BsParB proteins are ascribed, at least partly, to electrostatic interactions between opposite charges on the KCK tag and DNA backbone as evidenced by the enhanced fluorescence intensity on DNA and results of the ECE-tagged BsParB. However, we note that the KCK tag affected not only quantitative compaction rates but also qualitative behaviors of the protein against different nucleotide statuses and the presence of a *parS* sequence. Furthermore, in the absence of CTP, the lambda DNA compaction stopped before reaching the tether point with BsParB(WT)-KCK protein, while BsParB(WT) and KCK-BsParB(WT) proteins compacted DNA all the way to the tether point (Figure S2). Therefore, it is possible that KCK tags affect BsParB protein actions after its loading onto DNAs.

Previously, the R80A mutant of BsParB protein has been shown to be incapable of compacting DNA.^{23,43,46} However, slow but robust DNA compaction by BsParB(R80A) protein was observed in this study. Although both studies used the same assay, in our study, we supplemented magnesium ions to our buffer as a cofactor of CTP and used apyrase during our protein purification to remove residual CTPs. Since BsParB(R80A) is deficient in CTP hydrolysis,⁴¹ it is possible that CTPs were co-purified with BsParB(R80A) in the previous study.²³ Consistent with our speculation, in the absence of Mg²⁺ and the presence of CTP, BsParB(R80A)'s compaction rate was reduced dramatically (Figure S7), providing an explanation for the undetectable compaction by BsParB(R80A) in the previous study.

Although only the KCK-tagged BsParB proteins were tested with single-molecule DNA flow-stretching assay, our approach could be readily applicable to other DNA-binding proteins. For proteins capable of compacting DNA molecules, the DNA compaction rates of proteins containing desired tags (such as Halo, CLIP, SNAP, KCK, and sortase tags) need to be measured. DNA motion capture assay (a variant of the single-molecule DNA flow-stretching)^{14,21–23,51} can be also performed, and the comparison between untagged and tagged proteins will help determine the validity of the tagged protein. Once intact or minimally perturbed activity of the tagged proteins is confirmed, those tags can be labeled with a desired fluorescent dye, and the compaction rates can be measured again to detect any changes. In this case, the fluorescent dye on the protein and the QD at the end of the DNA must be spectrally distinct to allow the compaction rate measurements as we did in this and other studies.^{14,22} Our current study with KCK-tagged BsParB proteins shows that fluorescence labeling onto cysteine in the KCK tag with a charged fluorophore does not rescue the reduced protein's response to CTP. However, we do not rule out possibilities that for other DNA-binding proteins, or using a different fluorescent probe, the situation can be different. Our results urge researchers to thoroughly validate the use of tags and dyes for their single-molecule experiments.

In summary, deep understanding of any biological system requires both *in vitro* and *in vivo* approaches. Our study reveals

Cell Reports Methods

Resource



that the addition of short peptide tags may produce misleading *in vitro* results despite normal functionality *in vivo*. Additionally, our results raise a possibility that fluorescent dyes conjugated to a DNA-binding protein result in altered *in vitro* protein activities due to electrostatic interactions between charges on the fluorescent probe and those on the DNA backbone. Whenever adding a small amino acid tag is desired for *in vitro* experiments, careful controls must be performed to ensure that this does not perturb the activity of the protein. Here we show that the highly sensitive single-molecule DNA flow-stretching assay can be used as a powerful and efficient validation tool for modified proteins.

Limitations of the study

Here, using KCK tag on BsParB protein as a model system, we evaluate single-molecule DNA flow-stretching assay as an efficient and sensitive tool to assess the impact of small tags on protein action. While this study focuses on the methodology to validate protein tagging, the mechanism of BsParB action is being investigated in a separate study. Interestingly, although the KCK tags drastically altered ParB's action at *in vitro* single-molecule level, they did not change ParB's activity in *B. subtilis* live cells in any detectable way. These results imply that other cellular factors, such as the property of the cytoplasm and/or the biophysical aspects of the chromatin, make BsParB more tolerant to tagging in live cells than in the minimalist *in vitro* setups.

Here we have discovered and evaluated that small protein tags can lead to the change of protein property in single-molecule experiments. However, the scope of this study is limited to only BsParB protein and the KCK tags. It is desirable that other DNA-binding proteins with different fluorophore labeling platforms be investigated for future studies, such as site-specific labeling methodologies involving unnatural amino acids^{13,52,53} or aldehyde tags.⁵⁴

Finally, this DNA flow-stretching assay is applicable to proteins that have reasonable affinity to DNA. If the protein's DNA-binding affinity is too low, the fluorescence background might mask the signal from the DNA-bound proteins.

STAR★METHODS

Detailed methods are provided in the online version of this paper and include the following:

- KEY RESOURCES TABLE
- RESOURCE AVAILABILITY

- Lead contact
- Materials availability
- Data and code availability

- EXPERIMENTAL MODEL AND STUDY PARTICIPANT DETAILS

- METHOD DETAILS

- Plasmid constructions for *in vitro* assays
- Protein expression and purification
- DNA and quantum-dot preparations
- Nonspecific fluorescence BsParB protein labeling
- Fluorescent dye labeling on cysteine residue
- Single-molecule assays with unlabeled proteins

- Single-molecule assays with labeled proteins
- Fluorescence microscopy
- ChIP-seq
- Immunoblot analysis
- Plasmid construction for *in vivo* experiments

- QUANTIFICATION AND STATISTICAL ANALYSIS

SUPPLEMENTAL INFORMATION

Supplemental information can be found online at <https://doi.org/10.1016/j.crmeth.2023.100614>.

ACKNOWLEDGMENTS

We thank the Kim and Wang labs for discussions and support, Xheni Karabojë for assisting with ChIP-seq and microscopy experiments, Patrick Sheets for assisting with strain building, Candice Etson for providing the *E. coli* strain containing *parS*-lambda DNA, Thomas Graham for providing plasmids for BsParB wild-type and R80A mutant, Alan Grossman for strains and antibodies, and the Indiana University Center for Genomics and Bioinformatics for high-throughput sequencing. We thank Thomas Graham for reading the manuscript and providing insightful feedback. Support for this work comes from National Institutes of Health R01GM141242, R01GM143182, R01AI172822 (X.W.), and R35GM143093 (H.K.).

AUTHOR CONTRIBUTIONS

M.M. and H.K. purified proteins. M.M., B.G., B.S., and H.K. performed single-molecule experiments and analyzed data. L.E.W. constructed plasmids and strains and performed microscopy and immunoblot analysis. Z.R., Q.L., and X.W. performed ChIP-seq and analysis. X.W. designed, analyzed, and supervised the *in vivo* experiments. H.K. designed, analyzed data, and supervised the *in vitro* experiments. M.M. and L.E.W. contributed to writing the method sections of the paper. X.W. and H.K. wrote the paper with input from all authors.

DECLARATION OF INTERESTS

The authors declare no competing interests.

Received: April 26, 2023

Revised: July 28, 2023

Accepted: September 20, 2023

Published: October 12, 2023

REFERENCES

1. Toseland, C.P. (2013). Fluorescent labeling and modification of proteins. *J. Chem. Biol.* 6, 85–95. <https://doi.org/10.1007/s12154-013-0094-5>.
2. Zhang, J., Campbell, R.E., Ting, A.Y., and Tsien, R.Y. (2002). Creating new fluorescent probes for cell biology. *Nat. Rev. Mol. Cell Biol.* 3, 906–918. <https://doi.org/10.1038/nrm976>.
3. Fernández-Suárez, M., and Ting, A.Y. (2008). Fluorescent probes for super-resolution imaging in living cells. *Nat. Rev. Mol. Cell Biol.* 9, 929–943. <https://doi.org/10.1038/nrm2531>.
4. Arsić, A., Hagemann, C., Stajković, N., Schubert, T., and Nikić-Spiegel, I. (2022). Minimal genetically encoded tags for fluorescent protein labeling in living neurons. *Nat. Commun.* 13, 314. <https://doi.org/10.1038/s41467-022-27956-y>.
5. Crivat, G., and Taraska, J.W. (2012). Imaging proteins inside cells with fluorescent tags. *Trends Biotechnol.* 30, 8–16. <https://doi.org/10.1016/j.tibtech.2011.08.002>.
6. Giepmans, B.N.G., Adams, S.R., Ellisman, M.H., and Tsien, R.Y. (2006). The Fluorescent Toolbox for Assessing Protein Location and Function. *Science* 312, 217–224. <https://doi.org/10.1126/science.1124618>.

7. Lavis, L.D., and Raines, R.T. (2008). Bright ideas for chemical biology. *ACS Chem. Biol.* 3, 142–155. <https://doi.org/10.1021/cb700248m>.
8. Grimm, J.B., English, B.P., Chen, J., Slaughter, J.P., Zhang, Z., Revyakin, A., Patel, R., Macklin, J.J., Normanno, D., Singer, R.H., et al. (2015). A general method to improve fluorophores for live-cell and single-molecule microscopy. *Nat. Methods* 12, 244–250, 3 p following 250. <https://doi.org/10.1038/nmeth.3256>.
9. Gronemeyer, T., Godin, G., and Johnsson, K. (2005). Adding value to fusion proteins through covalent labelling. *Curr. Opin. Biotechnol.* 16, 453–458. <https://doi.org/10.1016/j.copbio.2005.06.001>.
10. Zheng, Q., Juette, M.F., Jockusch, S., Wasserman, M.R., Zhou, Z., Altman, R.B., and Blanchard, S.C. (2014). Ultra-stable organic fluorophores for single-molecule research. *Chem. Soc. Rev.* 43, 1044–1056. <https://doi.org/10.1039/c3cs60237k>.
11. Kremers, G.J., Gilbert, S.G., Cranfill, P.J., Davidson, M.W., and Piston, D.W. (2011). Fluorescent proteins at a glance. *J. Cell Sci.* 124, 157–160. <https://doi.org/10.1242/jcs.072744>.
12. Machado, J.H., Ting, R., Lin, J.Y., and Rodriguez, E.A. (2021). A self-labeling protein based on the small ultra-red fluorescent protein, smURFP. *RSC Chem. Biol.* 2, 1221–1226. <https://doi.org/10.1039/d1cb00127b>.
13. Laxman, P., Ansari, S., Gaus, K., and Goyette, J. (2021). The Benefits of Unnatural Amino Acid Incorporation as Protein Labels for Single Molecule Localization Microscopy. *Front. Chem.* 9, 641355. <https://doi.org/10.3389/fchem.2021.641355>.
14. Kim, H., and Loparo, J.J. (2016). Multistep assembly of DNA condensation clusters by SMC. *Nat. Commun.* 7, 10200. <https://doi.org/10.1038/ncomms10200>.
15. Zanetti-Domingues, L.C., Tynan, C.J., Rolfe, D.J., Clarke, D.T., and Martin-Fernandez, M. (2013). Hydrophobic Fluorescent Probes Introduce Artifacts into Single Molecule Tracking Experiments Due to Non-Specific Binding. *PLoS One* 8, e74200. <https://doi.org/10.1371/journal.pone.0074200>.
16. Sperling, R.A., Liedl, T., Duhr, S., Kudera, S., Zanella, M., Lin, C.A.J., Chang, W.H., Braun, D., and Parak, W.J. (2007). Size determination of (bio)conjugated water-soluble colloidal nanoparticles: A comparison of different techniques. *J. Phys. Chem. C* 111, 11552–11559. <https://doi.org/10.1021/jp070999d>.
17. Cai, E., Ge, P., Lee, S.H., Jeyifous, O., Wang, Y., Liu, Y., Wilson, K.M., Lim, S.J., Baird, M.A., Stone, J.E., et al. (2014). Stable small quantum dots for synaptic receptor tracking on live neurons. *Angew. Chem. Int. Ed. Engl.* 53, 12484–12488. <https://doi.org/10.1002/anie.201405735>.
18. Lee, J., Feng, X., Chen, O., Bawendi, M.G., and Huang, J. (2018). Stable, small, specific, low-valency quantum dots for single-molecule imaging. *Nanoscale* 10, 4406–4414. <https://doi.org/10.1039/c7nr08673c>.
19. Wang, Y., Cai, E., Rosenkranz, T., Ge, P., Teng, K.W., Lim, S.J., Smith, A.M., Chung, H.J., Sachs, F., Green, W.N., et al. (2014). Small quantum dots conjugated to nanobodies as immunofluorescence probes for nanometric microscopy. *Bioconjug. Chem.* 25, 2205–2211. <https://doi.org/10.1021/bc5004179>.
20. Lee, S.H., Jin, C., Cai, E., Ge, P., Ishitsuka, Y., Teng, K.W., de Thomaz, A.A., Nall, D., Baday, M., Jeyifous, O., et al. (2017). Super-resolution imaging of synaptic and Extra-synaptic AMPA receptors with different-sized fluorescent probes. *Elife* 6, e27744. <https://doi.org/10.7554/elife.27744>.
21. Kim, H., Yen, L., Wongpalee, S.P., Kirshner, J.A., Mehta, N., Xue, Y., Johnston, J.B., Burlingame, A.L., Kim, J.K., Loparo, J.J., and Jacobsen, S.E. (2019). The gene-silencing protein MORC-1 topologically entraps DNA and forms multimeric assemblies to cause DNA compaction. *Mol. Cell* 75, 700–710.e6. <https://doi.org/10.1016/j.molcel.2019.07.032>.
22. Kim, H., and Loparo, J.J. (2018). Observing Bacterial Chromatin Protein-DNA Interactions by Combining DNA Flow-Stretching with Single-Molecule Imaging. In *Bacterial Chromatin. Methods in Molecular Biology*, vol 1837, R. Dame, ed. (Humana Press), pp. 277–299. https://doi.org/10.1007/978-1-4939-8675-0_15.
23. Graham, T.G.W., Wang, X., Song, D., Etson, C.M., van Oijen, A.M., Rudner, D.Z., and Loparo, J.J. (2014). ParB spreading requires DNA bridging. *Genes Dev.* 28, 1228–1238. <https://doi.org/10.1101/gad.242206.114>.
24. Kath, J.E., Jergic, S., Heltzel, J.M.H., Jacob, D.T., Dixon, N.E., Sutton, M.D., Walker, G.C., and Loparo, J.J. (2014). Polymerase exchange on single DNA molecules reveals processivity clamp control of translesion synthesis. *Proc. Natl. Acad. Sci. USA* 111, 7647–7652. <https://doi.org/10.1073/pnas.1321076111>.
25. Kim, S., Blainey, P.C., Schroeder, C.M., and Xie, X.S. (2007). Multiplexed single-molecule assay for enzymatic activity on flow-stretched DNA. *Nat. Methods* 4, 397–399. <https://doi.org/10.1038/nmeth1037>.
26. Yardimci, H., Loveland, A.B., Habuchi, S., Van Oijen, A.M., and Walter, J.C. (2010). Uncoupling of Sister Replisomes during Eukaryotic DNA Replication. *Mol. Cell* 40, 834–840. <https://doi.org/10.1016/j.molcel.2010.11.027>.
27. Jensen, K.S., Pedersen, J.T., Winther, J.R., and Teilmann, K. (2014). The pKa value and accessibility of cysteine residues are key determinants for protein substrate discrimination by glutaredoxin. *Biochemistry* 53, 2533–2540. <https://doi.org/10.1021/bi4016633>.
28. Lobocki, M., Zakrzewska, M., Szlachcic, A., Krzysik, M.A., Sokolowska-Wedzina, A., and Otlewski, J. (2017). High-Yield Site-Specific Conjugation of Fibroblast Growth Factor 1 with Monomethylauristatin e via Cysteine Flanked by Basic Residues. *Bioconjug. Chem.* 28, 1850–1858. <https://doi.org/10.1021/acs.bioconjchem.7b00158>.
29. Parente, A., Merrifield, B., Geraci, G., and D'Alessio, G. (1985). Molecular Basis of Superactivity of Cysteine Residues 31 and 32 of Seminal Ribonuclease. *Biochemistry* 24, 1098–1104. <https://doi.org/10.1021/bi00326a005>.
30. Nawrocka, D., Krzysik, M.A., Opaliński, Ł., Zakrzewska, M., and Otlewski, J. (2020). Stable fibroblast growth factor 2 dimers with high pro-survival and mitogenic potential. *Int. J. Mol. Sci.* 21, 4108. <https://doi.org/10.3390/ijms21114108>.
31. Larson, A.G., Elnatan, D., Keenen, M.M., Trnka, M.J., Johnston, J.B., Burlingame, A.L., Agard, D.A., Redding, S., and Narlikar, G.J. (2017). Liquid droplet formation by HP1 α suggests a role for phase separation in heterochromatin. *Nature* 547, 236–240. <https://doi.org/10.1038/nature22822>.
32. Sallee, N.A., Rivera, G.M., Dueber, J.E., Vasilescu, D., Mullins, R.D., Mayer, B.J., and Lim, W.A. (2008). The pathogen protein EspFU hijacks actin polymerization using mimicry and multivalency. *Nature* 454, 1005–1008. <https://doi.org/10.1038/nature07170>.
33. Ginosyan, A.A., Grintsevich, E.E., and Reisler, E. (2019). Neuronal drebrin A directly interacts with mDia2 formin to inhibit actin assembly. *Mol. Biol. Cell* 30, 646–657. <https://doi.org/10.1091/mbc.E18-10-0639>.
34. Son, S., Takatori, S.C., Belardi, B., Podolski, M., Bakalar, M.H., and Fletcher, D.A. (2020). Molecular height measurement by cell surface optical profilometry (CSOP). *Proc. Natl. Acad. Sci. USA* 117, 14209–14219. <https://doi.org/10.1073/pnas.192262117>.
35. Hansen, S.D., and Mullins, R.D. (2010). VASP is a processive actin polymerase that requires monomeric actin for barbed end association. *J. Cell Biol.* 191, 571–584. <https://doi.org/10.1083/jcb.201003014>.
36. Van Den Ent, F., Johnson, C.M., Persons, L., De Boer, P., and Löwe, J. (2010). Bacterial actin MreB assembles in complex with cell shape protein RodZ. *EMBO J.* 29, 1081–1090. <https://doi.org/10.1038/embj.2010.9>.
37. Garner, E.C., Campbell, C.S., Weibel, D.B., and Mullins, R.D. (2007). Reconstitution of DNA Segregation Driven by Assembly of a Prokaryotic Actin Homolog. *Science* 315, 1270–1274. <https://doi.org/10.1126/science.1138527>.
38. Badrinarayanan, A., Le, T.B.K., and Laub, M.T. (2015). Bacterial chromosome organization and segregation. *Annu. Rev. Cell Dev. Biol.* 31, 171–199. <https://doi.org/10.1146/annurev-cellbio-100814-125211>.
39. Jalal, A.S.B., and Le, T.B.K. (2020). Bacterial chromosome segregation by the ParABS system. *Open Biol.* 10, 200097. <https://doi.org/10.1098/rsob.200097>.

Cell Reports Methods

Resource



40. Osorio-Valeriano, M., Altegoer, F., Steinchen, W., Urban, S., Liu, Y., Bange, G., and Thanbichler, M. (2019). ParB-type DNA Segregation Proteins Are CTP-Dependent Molecular Switches. *Cell* 179, 1512–1524.e15. <https://doi.org/10.1016/j.cell.2019.11.015>.
41. Soh, Y.M., Davidson, I.F., Zamuner, S., Basquin, J., Bock, F.P., Taschner, M., Veening, J.W., de Los Rios, P., Peters, J.M., and Gruber, S. (2019). Self-organization of parS centromeres by the ParB CTP hydrolase. *Science* 366, 1129–1133. <https://doi.org/10.1126/science.aay3965>.
42. Jalal, A.S., Tran, N.T., and Le, T.B. (2020). ParB spreading on DNA requires cytidine triphosphate in vitro. *Elife* 9, e53515–e53524. <https://doi.org/10.7554/elife.53515>.
43. Balaguer, F.d.A., Aicart-Ramos, C., Fisher, G.L., de Bragança, S., Martin-Cuevas, E.M., Pastrana, C.L., Dillingham, M.S., and Moreno-Herrero, F. (2021). CTP promotes efficient ParB-dependent DNA condensation by facilitating one-dimensional diffusion from pars. *Elife* 10, e67554. <https://doi.org/10.7554/elife.67554>.
44. Tisma, M., Panoukidou, M., Antar, H., Soh, Y.-M., Barth, R., Pradhan, B., Barth, A., Van Der Torre, J., Michieletto, D., Gruber, S., and Dekker, C. (2022). ParB proteins can bypass DNA-bound roadblocks via dimer-dimer recruitment. *Sci. Adv.* 8, esbn3299. <https://doi.org/10.1126/sciadv.abj3299>.
45. Antar, H., Soh, Y.-M., Zamuner, S., Bock, F.P., Anchimiuk, A., Rios, P.D.L., and Gruber, S. (2021). Relief of ParB autoinhibition by parS DNA catalysis and recycling of ParB by CTP hydrolysis promote bacterial centromere assembly. *Sci. Adv.* 7, esbj2854. <https://doi.org/10.1126/sciadv.abj2854>.
46. Song, D., Rodrigues, K., Graham, T.G.W., and Loparo, J.J. (2017). A network of cis and trans interactions is required for ParB spreading. *Nucleic Acids Res.* 45, 7106–7117. <https://doi.org/10.1093/nar/gkx271>.
47. Autret, S., Nair, R., and Errington, J. (2001). Genetic analysis of the chromosome segregation protein SPoOj of *Bacillus subtilis*: Evidence for separate domains involved in DNA binding and interactions with Soj protein. *Mol. Microbiol.* 41, 743–755. <https://doi.org/10.1046/j.1365-2958.2001.02551.x>.
48. Hoffman, M.T., Sheung, J., and Selvin, P.R. (2011). Fluorescence Imaging with One Nanometer Accuracy: In Vitro and In Vivo Studies of Molecular Motors. In Single Molecule Enzymology. Methods in Molecular Biology, vol 778, G. Mashanov and C. Batters, eds. (Humana Press), pp. 33–56. https://doi.org/10.1007/978-1-61779-261-8_4.
49. Bueno-Alejo, C.J., Santana Vega, M., Chaplin, A.K., Farrow, C., Axer, A., Burley, G.A., Dominguez, C., Kara, H., Paschalidis, V., Tubasum, S., et al. (2022). Surface Passivation with a Perfluoroalkane Brush Improves the Precision of Single-Molecule Measurements. *ACS Appl. Mater. Interfaces* 14, 49604–49616. <https://doi.org/10.1021/acsami.2c16647>.
50. Madariaga-Marcos, J., Pastrana, C.L., Fisher, G.L., Dillingham, M.S., and Moreno-Herrero, F. (2019). ParB dynamics and the critical role of the CTD in DNA condensation unveiled by combined force-fluorescence measurements. *Elife* 8, e43812. <https://doi.org/10.7554/elife.43812.001>.
51. Price, A.C., Pilkiewicz, K.R., Graham, T.G.W., Song, D., Eaves, J.D., and Loparo, J.J. (2015). DNA motion capture reveals the mechanical properties of DNA at the mesoscale. *Biophys. J.* 108, 2532–2540. <https://doi.org/10.1016/j.bpj.2015.04.022>.
52. Lee, K.J., Kang, D., and Park, H.S. (2019). Site-Specific Labeling of Proteins Using Unnatural Amino Acids. *Mol. Cells* 42, 386–396. <https://doi.org/10.14348/molcells.2019.0078>.
53. Elia, N. (2021). Using unnatural amino acids to selectively label proteins for cellular imaging: a cell biologist viewpoint. *FEBS J.* 288, 1107–1117. <https://doi.org/10.1111/febs.15477>.
54. Shi, X., Jung, Y., Lin, L.J., Liu, C., Wu, C., Cann, I.K.O., and Ha, T. (2012). Quantitative fluorescence labeling of aldehyde-tagged proteins for single-molecule imaging. *Nat. Methods* 9, 499–503. <https://doi.org/10.1038/nmeth.1954>.
55. Lin, D.C., Levin, P.A., and Grossman, A.D. (1997). Bipolar localization of a chromosome partition protein in *Bacillus subtilis*. *Proc. Natl. Acad. Sci. USA* 94, 4721–4726. <https://doi.org/10.1073/pnas.94.9.4721>.
56. Fujita, M. (2000). Temporal and selective association of multiple sigma factors with RNA polymerase during sporulation in *Bacillus subtilis*. *Gene Cell* 5, 79–88. <https://doi.org/10.1046/j.1365-2443.2000.00307.x>.
57. Youngman, P.J., Perkins, J.B., and Losick, R. (1983). Genetic transposition and insertional mutagenesis in *Bacillus subtilis* with *Streptococcus faecalis* transposon Tn917. *Proc. Natl. Acad. Sci. USA* 80, 2305–2309. <https://doi.org/10.1073/pnas.80.8.2305>.
58. Ireton, K., Gunther, N.W., and Grossman, A.D. (1994). spo0J is required for normal chromosome segregation as well as the initiation of sporulation in *Bacillus subtilis*. *J. Bacteriol.* 176, 5320–5329. <https://doi.org/10.1128/jb.176.17.5320-5329.1994>.
59. Lin, D.C., and Grossman, A.D. (1998). Identification and characterization of a bacterial chromosome partitioning site. *Cell* 92, 675–685. [https://doi.org/10.1016/S0092-8674\(00\)81135-6](https://doi.org/10.1016/S0092-8674(00)81135-6).
60. Edelstein, A.D., Tsuchida, M.A., Amodaj, N., Pinkard, H., Vale, R.D., and Stuurman, N. (2014). Advanced methods of microscope control using μManager software. *J. Biol. Methods* 1, e10. <https://doi.org/10.14440/jbm.2014.36>.
61. Schindelin, J., Arganda-Carreras, I., Frise, E., Kaynig, V., Longair, M., Pietzsch, T., Preibisch, S., Rueden, C., Saalfeld, S., Schmid, B., et al. (2012). Fiji: An open-source platform for biological-image analysis. *Nat. Methods* 9, 676–682. <https://doi.org/10.1038/nmeth.2019>.
62. Harwood, C.R., and Cutting, S.M. (1991). In Molecular Biological Methods for *Bacillus*, C.R. Harwood and S.M. Cutting, eds. (John Wiley).
63. Wang, X., Brandão, H.B., Le, T.B.K., Laub, M.T., and Rudner, D.Z. (2017). *Bacillus subtilis* SMC complexes juxtapose chromosome arms as they travel from origin to terminus. *Science* 355, 524–527. <https://doi.org/10.1126/science.aai8982.Bacillus>.
64. Wang, X., Le, T.B.K., Lajoie, B.R., Dekker, J., Laub, M.T., and Rudner, D.Z. (2015). Condensin promotes the juxtaposition of DNA flanking its loading site in *Bacillus subtilis*. *Genes Dev.* 29, 1661–1675. <https://doi.org/10.1101/gad.265876.115>.
65. le Cessie, S., Goeman, J.J., and Dekkers, O.M. (2020). Who is afraid of non-normal data? Choosing between parametric and non-parametric tests. *Eur. J. Endocrinol.* 182, E1–E3. <https://doi.org/10.1530/EJE-19-0922>.

STAR★METHODS

KEY RESOURCES TABLE

REAGENT or RESOURCE	SOURCE	IDENTIFIER
Antibodies		
Sheep Anti-Digoxigenin Fab fragments Antibody, Unconjugated	Roche	Cat#11214667001; RRID: AB_514494
Anti-ParB	Lin et al. ⁵⁵	N/A
Anti-SigA	Fujita ⁵⁶	N/A
Immun-Star Goat Anti-Rabbit (GAR)-HRP Conjugate	Bio-Rad	Cat#1705046; RRID: AB_11125757
Bacterial and virus strains		
5-alpha Competent <i>E. coli</i>	New England Biolabs	Cat#C2987H
Rosetta 2(DE3)pLysS Competent Cells	EMD Millipore	Cat#71403
<i>pelB::Psoj-mgfpmut3-spo0J WT (ΔparS) tet, Δspo0J::spec, sacA::hbs-mcherry kan</i>	Graham et al. ²³	BWX2213 (BDR2798)
<i>pelB::Psoj-mgfpmut3-spo0J-R80A (ΔparS) tet, Δspo0J::spec, sacA::hbs-mcherry kan</i>	Graham et al. ²³	BWX2214 (BDR2799)
<i>pelB::Psoj-soj-spo0J-R80A (Δpars) cat, Δ(soj spo0J)::spec</i>	This paper	BWX2032
<i>pelB::Psoj-soj-spo0J-WT (ΔparS) cat, Δ(soj spo0J)::spec</i>	This paper	BWX2034
<i>pelB::Psoj-mgfpmut3-spo0J(ΔparS)-KCK cat, Δspo0J::spec, sacA::hbs-mcherry kan</i>	This paper	BWX5438
<i>pelB::Psoj-spo0J(ΔparS)-mgfpmut3 tet, Δspo0J::spec, sacA::hbs-mcherry kan</i>	This paper	BWX5440
<i>pelB::Psoj-KCK-spo0J(ΔparS)-mgfpmut3 tet, Δspo0J::spec, sacA::hbs-mcherry kan</i>	This paper	BWX5442
<i>pelB::Psoj-soj-spo0J(ΔparS)-KCK cat, Δ(soj spo0J)::spec</i>	This paper	BWX5444
<i>pelB::Psoj-spo0J-R80A(ΔparS)-mgfpmut3 tet, Δspo0J::spec, sacA::hbs-mcherry kan</i>	This paper	BWX5452
<i>pelB::Psoj-KCK-spo0J-R80A(ΔparS)-mgfpmut3 tet, Δspo0J::spec, sacA::hbs-mcherry kan</i>	This paper	BWX5460
<i>pelB::Psoj-mgfpmut3-spo0J-R80A(ΔparS)-KCK cat, Δspo0J::spec, sacA::hbs-mcherry kan</i>	This paper	BWX5464
<i>pelB::Psoj-KCK-spo0J(ΔparS) tet, Δspo0J::spec</i>	This paper	BWX5466
<i>pelB::Psoj-KCK-spo0J-R80A(ΔparS) tet, Δspo0J::spec</i>	This paper	BWX5468
<i>pelB::Psoj-soj-spo0J-R80A(ΔparS)-KCK cat, Δ(soj spo0J)::spec</i>	This paper	BWX5470
<i>pelB::Psoj-ECE-spo0J(ΔparS) tet, Δspo0J::spec</i>	This paper	BWX5572
<i>pelB::Psoj-ECE-spo0J-R80A(ΔparS) tet, Δspo0J::spec</i>	This paper	BWX5574
<i>pelB::Psoj-ECE-spo0J(ΔparS)-mgfpmut3 tet, Δspo0J::spec, sacA::hbs-mcherry kan</i>	This paper	BWX5576
<i>pelB::Psoj-ECE-spo0J-R80A(ΔparS)-mgfpmut3 tet, Δspo0J::spec, sacA::hbs-mcherry kan</i>	This paper	BWX5578
wild type	Youngman et al. ⁵⁷	PY79
<i>Δspo0J::spec, trpC2, pheA1</i>	Ireton et al. ⁵⁸	AG1468
<i>Δ(soj spo0J)::spec, trpC2, pheA1</i>	Ireton et al. ⁵⁸	AG1505
<i>spo0J (ΔparS), trpC2, pheA1</i>	Lin et al. ⁵⁹	DCL468
Chemicals, peptides, and recombinant proteins		
T4 polynucleotide kinase (PNK)	New England Biolabs	Cat#M0201S
Apyrase	New England Biolabs	Cat#M3098L
Neutravidin	Thermo Fisher Scientific	Cat#31000
Cytidine 5'-triphosphate (CTP) disodium salt	Millipore Sigma	Cat#C1506; CAS: 36051-68-0

(Continued on next page)

Cell Reports Methods

Resource



Continued

REAGENT or RESOURCE	SOURCE	IDENTIFIER
CTP γ S	Jena Bioscience	Custom-synthesized
Sulfo-Cyanine3 NHS ester	Lumiprobe	Cat#11320
Alexa Fluor 647 C ₂ maleimide	Thermo Fisher Scientific	Cat#A20347
TCEP (tris(2-carboxyethyl)phosphine)	Thermo Fisher Scientific	Cat#77720
cComplete Mini EDTA-free Protease Inhibitor Cocktail	Roche	Cat#04 693 159 001
Protease inhibitor cocktail	Millipore Sigma	Cat#P8340
Universal Nuclease for Cell Lysis	Thermo Fisher Scientific	Cat#88701
Ni-NTA agarose	Qiagen	Cat#30230
InstantBlue Coomassie protein stain	Abcam	Cat#ISB1L
Qdot 605 ITK Amino (PEG) Quantum Dots	Thermo Fisher Scientific	Cat#Q21501MP
Superdex 200 Prep Grade	Cytiva	Cat#17104301
(3-Aminopropyl)triethoxysilane	Millipore Sigma	Cat#A3648; CAS: 919-30-2
mPEG-Succinimidyl Valerate, MW 5,000	Laysan Bio	Cat#MPEG-SVA-5000-1g
Biotin-PEG-SVA, MW 5,000	Laysan Bio	Cat#Biotin-PEG-SVA-5000-100mg
Western Lightning ONE Femto, Chemiluminescent Substrate	Perkin Elmer	Cat#NEL1034001
Formaldehyde 37%	Sigma	Cat#F8775
Ready-Lyse Lysozyme	Epicentre	Cat#R1802M
Proteinase inhibitor cocktail for immunoblotting	Sigma-Aldrich	Cat#P-8340
10x Casein solution	Vector Laboratories	Cat#SP-5020-250
Bovine serum albumin (BSA)	New England Biolabs	Cat#B9000S
Critical commercial assays		
NEBuilder HiFi DNA Assembly Master Mix	New England Biolabs	Cat#E2621S
Ultra II DNA Library Prep Kit for Illumina	New England Biolabs	Cat#E7645
Deposited data		
ChIP data	Gene Expression Omnibus	Accession#GSE212751; https://www.ncbi.nlm.nih.gov/geo/query/acc.cgi?acc=GSE212751
Oligonucleotides		
Oligonucleotides used in this study	This paper	See Tab 8 in Data S1 .
Recombinant DNA		
His6-SUMO-BsParB(WT)-KCK amp	This paper	m0067
His6-SUMO-BsParB(R80A)-KCK amp	This paper	m0069
<i>pelB::Psoj-mgfpmut3-spo0J(ΔparS) tet</i>	Graham et al. ²³	pWX563
<i>pelB::Psoj-mgfpmut3-spo0J(ΔparS)-KCK cat</i>	Graham et al. ²³	pWX611
<i>pelB::Psoj-soj-spo0J(ΔparS)-KCK cat</i>	Graham et al. ²³	pWX612
<i>pelB::Psoj-spo0J(ΔparS)-mgfpmut3 tet</i>	This paper	pWX1092
<i>pelB::Psoj-KCK-spo0J(ΔparS)-mgfpmut3 tet</i>	This paper	pWX1093
<i>pelB::Psoj-mgfpmut3-spo0J-R80A(ΔparS)-KCK cat</i>	This paper	pWX1103
<i>pelB::Psoj-spo0J-R80A(ΔparS)-mgfpmut3 tet</i>	This paper	pWX1104
<i>pelB::Psoj-KCK-spo0J-R80A(ΔparS)-mgfpmut3 tet</i>	This paper	pWX1105
<i>pelB::Psoj-soj-spo0J-R80A(ΔparS)-KCK cat</i>	This paper	pWX1106
<i>pelB::Psoj-KCK-spo0J(ΔparS) tet</i>	This paper	pWX1107
<i>pelB::Psoj-KCK-spo0J-R80A(ΔparS) tet</i>	This paper	pWX1108
<i>pelB::Psoj-ECE-spo0J(ΔparS) tet</i>	This paper	pWX1167
<i>pelB::Psoj-ECE-spo0J-R80A(ΔparS) tet</i>	This paper	pWX1168
<i>pelB::Psoj-ECE-spo0J(ΔparS)-mgfpmut3 tet</i>	This paper	pWX1169
<i>pelB::Psoj-ECE-spo0J-R80A(ΔparS)-mgfpmut3 tet</i>	This paper	pWX1170
<i>pelB::Psoj-soj-spo0J(ΔparS) cat</i>	Graham et al. ²³	pNS069

(Continued on next page)

Continued

REAGENT or RESOURCE	SOURCE	IDENTIFIER
His6-SUMO-BsParB(WT) <i>amp</i>	Graham et al. ²³	pTG011 (=m0041)
<i>pelB::Psoj-spo0J-R80A(ΔparS)-mgfpmut3 tet</i>	This paper	pWX1104
His6-SUMO-BsParB(R80A) <i>amp</i>	Graham et al. ²³	pTG037 (=m0042)
His6-SUMO-KCK-BsParB(WT) <i>amp</i>	Graham et al. ²³	pTG042 (=m0043)
His6-SUMO-KCK-BsParB(R80A) <i>amp</i>	Graham et al. ²³	pTG044 (=m0044)
His6-SUMO-ECE-BsParB(WT) <i>amp</i>	This paper	m0064
His6-SUMO-BsParB(WT)-KCK <i>amp</i>	This paper	m0067
His6-SUMO-BsParB(R80A)-KCK <i>amp</i>	This paper	m0069
His6-SUMO-ECE-BsParB(R80A) <i>amp</i>	This paper	m0070
<i>pelB::Psoj-soj-spo0J-R80A(ΔparS) cat</i>	Graham et al. ²³	pTG122
Software and algorithms		
MicroManager	Edelstein et al. ⁶⁰	https://micro-manager.org
Fiji	Schindelin et al. ⁶¹	https://imagej.net/Fiji
MATLAB codes used in single-molecule data analyses	Kim et al. ¹⁴	N/A
MetaMorph	Molecular Devices	https://www.moleculardevices.com/
AlphaView	ProteinSimple	https://proteinsimple.jp/imaging-crunch-some-numbers
CLC Genomics Workbench	Qiagen	https://www.qiagen.com/us/products/discovery-and-translational-research/next-generation-sequencing/informatics-and-data/analysis-and-visualization/clc-genomics-workbench
Other		
Lambda DNA (<i>dam</i> -)	New England Biolabs	Cat#N3013S
Micro Bio-Spin P-30 Gel Columns, Tris Buffer	Bio-Rad	Cat#7326223
IX-83 total internal reflection fluorescence (TIRF) microscope	Olympus (Evident)	https://www.olympus-lifescience.com/
Ti2 microscope	Nikon instruments	https://www.microscope.healthcare.nikon.com/
OptoSplit II	Cairn Research	https://www.cairn-research.co.uk/product/optosplit-ii/
T660lpxrxt (Dichroic)	Chroma Technology Corp.	https://www.chroma.com/
ET705/72m (Emission filter)	Chroma Technology Corp.	https://www.chroma.com/
ET585/65m (Emission filter)	Chroma Technology Corp.	https://www.chroma.com/
Q800R2 water bath sonicator	Qsonica	https://www.sonicator.com/
ProteinSimple Fluorchem R system	Bio-Techne	https://www.bio-techne.com/p/imaging/fluorchem-r-system_92-15313-00
UVP UVsolo touch gel documentation system	Analytik Jena	https://www.analytik-jena.com/
NextSeq 500 System WGS Solution	Illumina	https://www.illumina.com/
Protein A magnetic Sepharose beads	Cytiva	Cat#28951378
4-15% Mini-PROTEAN TGX Precast Protein Gels	Bio-Rad	Cat#4561086
4-20% Mini-PROTEAN TGX Precast Protein Gels	Bio-Rad	Cat#4561096
Trans-Blot Turbo Mini 0.2 µm PVDF Transfer Packs	Bio-Rad	Cat#1704156

RESOURCE AVAILABILITY

Lead contact

Further information and requests for resources should be directed to and will be fulfilled by the lead contact, HyeongJun Kim (hyeongjun.kim@utrgv.edu).

Materials availability

Bacterial strains and plasmids generated in this study are available from the corresponding authors upon request.

Cell Reports Methods

Resource



Data and code availability

- ChIP-seq data that support the findings of this study have been deposited in the Gene Expression Omnibus with accession no. GSE212751 (<https://www.ncbi.nlm.nih.gov/geo/query/acc.cgi?acc=GSE212751>). Next-generation sequencing samples used in this study can be found in Tab 9 in [Data S1](#). A list of figures that have associated raw data can be found from Tabs 6 and 9 in [Data S1](#).
- Single-molecule analysis data can be found in Tabs 1–5 in [Data S1](#).
- The MATLAB codes used in single-molecule data are available from our previous publication.¹⁴ Alternatively, the codes will be available from the corresponding author (H.K.) upon request.
- Any additional information required to reanalyze the data reported in this paper is available from the [lead contact](#) upon request.

EXPERIMENTAL MODEL AND STUDY PARTICIPANT DETAILS

Bacillus subtilis strains were derived from the prototrophic strain PY79.⁵⁷ *B. subtilis* strains were generated by successive transformations of plasmids or genomic DNA. Cells were grown in defined rich Casein Hydrolysate (CH) medium⁶² at 37°C. Strains used in this study can be found in Tab 6 in [Data S1](#) and the [Key resources table](#).

METHOD DETAILS

Plasmid constructions for *in vitro* assays

Plasmids harboring coding sequences of His6-SUMO-BsParB(WT) (pTG011),²³ His6-SUMO-KCK-BsParB(WT) (pTG042),²³ His6-SUMO-BsParB(R80A) (pTG037),²³ and His6-SUMO-KCK-BsParB(R80A) (pTG044)²³ were generous gifts from Thomas Graham. Site-directed mutagenesis were performed to generate plasmids harboring coding sequences of His6-SUMO-BsParB(WT)-KCK (m0067) and His6-SUMO-BsParB(R80A)-KCK (m0069) using oHK050F and oHK050R as primers. The plasmid harboring coding sequences of His6-SUMO-ECE-BsParB(WT) (m0064) were generated using oHK048F and oHK048R as primers and m0043 as a substrate. Contrary to other plasmids, the plasmid harboring coding sequences of His6-SUMO-ECE-BsParB(R80A) (m0070) was generated by following the vendor-supplied NEBuilder HiFi DNA Assembly Master Mix (NEB E2621S, Ipswich, MA) protocol. First, the His6-SUMO-BsParB(WT) plasmid (pTG011 = m0041) was linearized and the majority of SUMO-BsParB(WT) coding sequences were removed by PCR using oHK038F and oHK038R as primers. Then, gfHK009 and gfHK010 were used as gene fragments with both containing 23 bp overlaps. After NEBuilder HiFi DNA assembly, NEB 5-alpha competent *E. coli* cells (NEB C2987H, Ipswich, MA) were transformed with the reaction mixture. The sequences were confirmed using T7, oHK023, oHK024, oHK025, and oHK026 oligos. See Tabs 7 and 8 in [Data S1](#) for the list of plasmids used in *in vitro* assays and the oligonucleotide sequences, respectively.

Protein expression and purification

Rosetta2(DE3)pLysS competent cells (EMD Millipore, Burlington, MA) transformed with a plasmid were cultured overnight at 37°C in the presence of 100 µg/mL ampicillin and 20 µg/mL chloramphenicol. 1 L of LB medium with 80 µg/mL ampicillin was inoculated with the overnight culture and grown at 37°C until the OD₆₀₀ reached 0.4–0.6. Protein expression was induced with 500 µM isopropyl-β-D-thiogalactoside (IPTG), and the culture was shaken at 30°C for an additional 4 h. The cells were harvested by centrifugation at 4°C. The cell pellets were resuspended in PBS buffer and spun at 5,000 g. They were resuspended in ParB lysis buffer (20 mM Tris, pH 8.0, 1 M NaCl, 50 mM imidazole, 5 mM 2-mercaptoethanol), supplemented with 0.1 mM phenylmethylsulfonyl fluoride (PMSF) and a protease inhibitor cocktail (Roche, Basel, Switzerland) (Total volume: 45 mL), and flash-frozen. BsParB proteins were purified based on a two-step tandem purification method as previously described²³ but with some modifications. Briefly, after thawing the harvested cells, additional 0.9 mM PMSF (total 1.0 mM PMSF), 50 mg/mL lysozyme, 3 µL of universal nuclease (Thermo Fisher Scientific 88701, Waltham, MA), and 5 mM 2-mercaptoethanol were added, and it was left in ice for 30 min. Cells were lysed by sonification and centrifuged twice in an FA-6x50 rotor: first at 11,000 g for 30 min, then at 20,133 g for 30 min. The clarified supernatant was incubated with Ni-NTA agarose beads (Qiagen, Hilden, Germany) for 1 h in the presence of 1 unit of apyrase (NEB, Ipswich, MA) and 5 mM MgCl₂, to help minimize cellular NTPs that may otherwise be co-purified, and 1 tablet of cComplete Mini EDTA-free protease inhibitor cocktail (Roche, Basel, Switzerland). The Ni-NTA agarose resin was washed with lysis buffer (supplemented with 5 mM MgCl₂) followed by ParB salt-reduction buffer (20 mM Tris, pH 8.0, 350 mM NaCl, 50 mM imidazole, 5 mM MgCl₂, 5 mM 2-mercaptoethanol). The proteins were manually eluted ten times with 1.5 mL of ParB elution buffer (20 mM Tris, pH 8.0, 350 mM NaCl, 250 mM imidazole, 5 mM MgCl₂, 5 mM 2-mercaptoethanol).

The peak fractions of ParB protein were pooled and treated with His6-Ulp1 protease to remove the N-terminal His6-SUMO tag.²³ The pooled proteins and His6-Ulp1 protease were dialyzed together overnight at 4°C against ParB dialysis/storage 1 buffer (20 mM Tris, pH 8.0, 350 mM NaCl, 10 mM imidazole, 5 mM 2-mercaptoethanol, 1 mM MgCl₂, 10% glycerol). After centrifuging the dialyzed proteins at maximum speed for 10 min, the supernatant was allowed to interact with the Ni-NTA resin for at least 1 h at 4°C. Then, the flowthrough was collected. 0.5 mL of the ParB dialysis/storage 1 buffer to the Ni-NTA resin column was added multiple times, and the eluents were collected. Running an SDS-polyacrylamide (SDS-PAGE) gel indicated that the flowthrough and the eluent fractions

contained ParB protein, while the cleaved His6-SUMO and His6-Ulp1 remained in the resin. The flowthrough and the peak fractions were pooled and dialyzed against ParB dialysis/storage 2 buffer (20 mM Tris, pH 8.0, 350 mM NaCl, 10% glycerol), where 5 mM 2-mercaptoethanol was included in case of KCK-tagged protein purifications. The protein concentration was measured by a NanoDrop One spectrophotometer (Thermo Scientific, Waltham, MA) using 32.58 (kDa) and 7,450 ($M^{-1} cm^{-1}$) as its molecular weight and extinction coefficient, respectively. The purified proteins (Figure S1A) were run on a 4–15% precast polyacrylamide gel (Bio-Rad, Hercules, CA) with Tris/Glycine/SDS running buffer (Bio-Rad, Hercules, CA). InstantBlue Coomassie protein stain (Abcam, Cambridge, United Kingdom) was used to stain for the polyacrylamide gel. The gel image was obtained using UV-Vis solo touch gel documentation system (Analytik Jena, Jena, Germany) and provided in the Figure S1A without any image processing.

DNA and quantum-dot preparations

One end of bacteriophage lambda DNA (or *parS* DNA²³) was labeled with a biotin to tether the DNA onto the single-molecule microfluidic flow cell, and the other end was labeled with a digoxigenin to attach a quantum dot (Figure 1A) as previously described.^{14,22} Briefly, Lambda-BL1Biotin and Lambda-Dig2 oligos (Tab 8 in Data S1) were treated with T4 polynucleotide kinase (PNK) (NEB, Ipswich, MA) for phosphorylation at 37°C for 1 h. A 15-fold molar excess of the phosphorylated Lambda-BL1Biotin oligo was introduced for annealing to a 12-base 5' single-stranded overhang on one end of lambda DNA (or *parS* DNA²³). The mixture of DNA and oligo was incubated at 65°C for 10 min and slowly cooled down, and then ligated by T4 ligase for 2 h at room temperature. The other end of the lambda DNA (or *parS* DNA) was tagged with a digoxigenin by supplementing a 60-fold molar excess of the phosphorylated Lambda-Dig2 oligo at 45°C. After 30-min incubation, the mixture was slowly back to room temperature followed by a 2-h ligation step at room temperature. Since the sequences of Lambda-BL1Biotin and Lambda-Dig2 oligos are complementary to each other, it is important to remove unreacted excess oligos. After running a 0.4% agarose gel overnight at 4°C, the desired DNA band was excised and put into a dialysis tube. Applying an electric field allowed DNAs to leave the excised agarose gel, but DNAs were confined to the dialysis tube volume. DNAs were collected, and ethanol precipitation was performed to recover doubly-tagged lambda DNAs (or *parS* DNAs) in EB buffer (10 mM Tris-Cl, pH 8.5).

As we previously did,^{14,21,22} anti-digoxigenin antibody-conjugated quantum dot 605 (Invitrogen, Waltham, MA) was prepared following Invitrogen's Qdot 605 antibody conjugation kit (Q22001MP) manual. However, since this kit was discontinued, all the kit components were separately purchased including Qdot 605 ITK amino (PEG) quantum dots (Invitrogen Q21501MP) and superdex 200 (prep grade) (Cytiva 17104301). For the antibody, anti-digoxigenin fab fragments (Roche 11214667001, Basel, Switzerland) were used.

Nonspecific fluorescence BsParB protein labeling

BsParB(WT) and BsParB(R80A) proteins were incubated with sulfo-Cyanine3 NHS ester dye (Lumiprobe 11320, Hunt Valley, MD) at 4°C overnight. Labeled protein was separated from free dye using Micro Bio-Spin P-30 gel columns (Bio-Rad 7326223, Hercules, CA). Each labeled protein and Cyanine3 dye concentrations were measured three times using Nanodrop, and the averaged values were used as final concentrations. The protein labeling efficiencies were 21.8%, 23.4%, 19.7%, 30.1%, 32.0%, and 30.0% for BsParB(WT), KCK-BsParB(WT), BsParB(WT)-KCK, BsParB(R80A), KCK-BsParB(R80A), and BsParB(R80A)-KCK, respectively. These numbers correspond to about 0.4 and 0.6 Cyanine3 dyes per each BsParB wild-type and R80A mutant protein dimers, respectively.

Fluorescent dye labeling on cysteine residue

The KCK-BsParB(WT) protein had been stored in a buffer containing 5 mM 2-mercaptoethanol, which can interfere maleimide dye labeling. First, using Micro Bio-Spin P-30 gel columns (Bio-Rad 7326223, Hercules, CA), the buffer was exchanged into a new buffer containing 30 μM tris(2-carboxyethyl)phosphine (TCEP) (Thermo Fisher Scientific 77720, Waltham, MA) devoid of 2-mercaptoethanol (20 mM Tris-base, pH 8.0; 10% glycerol; 350 mM NaCl; 30 μM TCEP). After determining the protein concentration, we added 5-fold molar excess of Alexa Fluor C₂ maleimide dye (Thermo Fisher Scientific A20347, Waltham, MA) and incubated it at 4°C overnight. The labeled protein was separated from unreacted dye via Micro Bio-Spin P-30 gel columns (Bio-Rad 7326223, Hercules, CA) using a buffer that contains 20 mM Tris-base, pH 8.0, 10% glycerol, 350 mM NaCl, and 5 mM 2-mercaptoethanol. The protein and the labeled dye concentrations were measured using 283,000 ($cm^{-1} M^{-1}$), 651 nm, 0.00, and 0.03 for the Alexa 647 extinction coefficient (vendor supplied value for the Lot number 2633288), corresponding wavelength, the correction factor at 260 nm, and the correction factor at 280 nm, respectively. The Alexa 647 maleimide labeling efficiency was 74.7% implying that each dimer has about 1.5 labeled Alexa 647 dyes. In parallel with these procedures, unlabeled protein sample was also prepared through a mock reaction without the Alexa Fluor 647 maleimide dye.

Single-molecule assays with unlabeled proteins

Surface-passivated coverglasses were prepared by aminopropyl silanization (Millipore Sigma A3648, St. Louis, MO) and PEGylation (PEG: polyethylene glycol) (Laysan Bio, Arab, AL) as previously described.^{14,22} A microfluidic flow cell was constructed from a quartz plate (Technical Glass Product, Paineville, OH) adhered to the PEGylated coverglass via double-sided tape (Grace Bio-Labs, Bend, OR) with rectangular cuts that make up the flow cell channels. Inlet and outlet tubing were inserted through holes on the quartz plate and made air-tight with epoxy.^{14,22} In-depth description of single-molecule flow-stretching assays was already provided in previous

publications.^{14,21,22} Briefly, about 4% of the PEG on the surface-passivated coverglass contains biotins that serve as a neutravidin binding platform. Pre-mixed quantum dot-labeled biotinylated lambda DNA (or *parS* DNA) was introduced to allow the DNA surface tethering. For experiments with labeled proteins, quantum dot incubation with biotinylated DNA is omitted. After washing unbound DNAs and quantum dots, an intended concentration of BsParB protein was flowed in (with and without nucleotides). Unless otherwise stated, the imaging buffer composition was 10 mM Tris, pH 7.5, 100 mM NaCl, and 2.5 mM MgCl₂. For the experiments without magnesium ions, the 2.5 mM MgCl₂ was omitted. CTPγS was custom-synthesized (Jena Bioscience, Jena, Germany). The single-molecule imaging was performed on a semi-custom microscope with a 532-nm laser (Coherent, Santa Clara, CA) built upon the IX-83 total internal reflection fluorescence (TIRF) microscope (Evident Scientific, Olympus, Waltham, MA). The images were recorded every 200 ms with 100-millisecond exposure time using the Micro-Manager software.⁶⁰ Regions-of-interest (ROIs) of DNA compaction events were determined using ImageJ (FIJI) software,⁶¹ and the positions of quantum dots as a function of time were determined by Gaussian-fitting-based custom-written MATLAB software codes.¹⁴

Single-molecule assays with labeled proteins

After quantum dot (QD)-labeled DNAs are tethered, unbound QD-DNAs were washed away by flowing imaging buffer supplemented with 0.05x casein (Vector Laboratories, Newark, CA; stock concentration: 10x) and 0.2 mg/mL bovine serum albumin (BSA) (New England Biolabs, Ipswich, MA). For the experiments with Alexa Fluor 647 maleimide-labeled protein, after 2-min incubation, imaging buffer (without casein and BSA) was flowed in to remove casein and BSA from the microfluidic flow cell channel. Alexa 647-KCK-BsParB(WT) protein was diluted to 50 nM in the imaging buffer (without casein and BSA) and applied to the flow cell at 50 μL/min. To separately observe quantum dot 605 on DNA and Alexa 647-labeled proteins, OptoSplit II image splitter (Cairn Research, Faversham, United Kingdom) was placed between the microscope and the EMCCD. T660pxrxt, ET585/65m, and ET705/72m (Chroma Technology, Bellows Falls, VT) are dichroic, emission filters for quantum dot 605 and Alexa Fluor 647, respectively, used in the OptoSplit II. For the experiments with Cyanine3 NHS ester-labeled proteins, after 2-min incubation, imaging buffer supplemented with 0.2 mg/mL BSA was flowed in. The proteins were diluted to 30 nM in the imaging buffer supplemented with 0.2 mg/mL BSA to further minimize nonspecific bindings and flowed in into the flow cell at 50 μL/min.

Fluorescence microscopy

Fluorescence microscopy was performed using a Nikon Ti2 microscope (Nikon Instruments, Melville, NY) equipped with Plan Apo 100x/1.45NA phase contrast oil objective and an sCMOS camera. Images were cropped and adjusted using MetaMorph software. Final figure preparation was performed in Adobe Illustrator.

ChIP-seq

Chromatin immunoprecipitation (ChIP) was performed as described previously.^{63,64} Briefly, cells were crosslinked using 3% formaldehyde for 30 min at room temperature and then quenched using 125 mM glycine, washed using PBS, and lysed using lysozyme. Crosslinked chromatin was sheared to an average size of 250 bp by sonication using Qsonica Q800R2 water bath sonicator. The lysate was precleared using Protein A magnetic beads (GE Healthcare/Cytiva 28951378, Marlborough, MA) and was then incubated with anti-ParB antibodies⁵⁵ overnight at 4°C. The next day, the lysate was incubated with Protein A magnetic beads for 1h at 4°C. After washes and elution, the immunoprecipitate was incubated at 65°C overnight to reverse the crosslinks. The DNA was further treated with RNaseA, Proteinase K, extracted with PCI, resuspended in 100 μL EB and used for library preparation with the NEBNext Ultra II kit (E7645). The library was sequenced using Illumina NextSeq500 (Illumina, San Diego, CA) at IU Center for Genomics and Bioinformatics. The sequencing reads were mapped to *B. subtilis* PY79 genome (NCBI Reference Sequence NC_022898.1) using CLC Genomics Workbench (Qiagen, Hilden, Germany). We note that the genome coordinate of this genome is shifted compared to the *B. subtilis* 168 genome (NC000964) used in our previous study.²³ Sequencing reads were normalized by the total number of reads, plotted and analyzed using R. Next-generation sequencing samples used in this study can be found in Tab 9 in Data S1.

Immunoblot analysis

Exponentially growing cells were collected and resuspended in lysis buffer (20 mM Tris pH 7.0, 1 mM EDTA, 10 mM MgCl₂, 1 mg/mL lysozyme, 10 μg/mL DNase I, 100 μg/mL RNase A, 1 mM PMSF and 1% proteinase inhibitor cocktail (Millipore Sigma, P8340, St. Louis, MO) to a final OD₆₀₀ of 10 for equivalent loading. The cell suspensions were incubated at 37°C for 10 min for lysozyme treatment, followed by the addition of an equal volume of 2x Laemmli Sample Buffer (Bio-Rad 1610737, Hercules, CA) containing 10% β-Mercaptoethanol. Samples were heated for 15 min at 65°C prior to loading. Proteins were separated by precast 4–20% polyacrylamide gradient gels (Bio-Rad 4561096, Hercules, CA) and electroblotted onto mini PVDF membranes using Bio-Rad Transblot Turbo system and reagents (Bio-Rad 1704156, Hercules, CA). The membranes were blocked in 5% nonfat milk in phosphate-buffered saline (PBS) with 0.5% Tween 20, then probed with anti-ParB (1:5000)⁵⁵ or anti-SigA (1:10,000)⁵⁶ diluted into 3% BSA in 1x PBS-0.05% Tween 20. Primary antibodies were detected using Immun-Star horseradish peroxidase-conjugated goat anti-rabbit antibodies (Bio-Rad 1705046, Hercules, CA) and Western Lightning Plus ECL chemiluminescence reagents as described by the manufacturer (PerkinElmer NEL1034001, Waltham, MA). The signal was captured using ProteinSimple Fluorchem R system (Bio-Techne, Minneapolis, MN). The intensity of the bands was quantified using ProteinSimple AlphaView software.

Plasmid construction for *in vivo* experiments

The list of plasmids can be found in Tab 7 in [Data S1](#).

pWX1092 [*pelB::Psoj-spo0J(ΔparS)-mgfpmut3 tet*] was constructed by an isothermal assembly reaction containing three fragments: 1) pWX516 digested with HindIII and BamHI, and gel purified; 2) *spo0J (ΔparS)* amplified from pWX563²³ using oWX2974 and oWX2975; 3) *mgfpmut3* amplified from pWX563²³ using oWX2976 and oWX2977. pWX516 contains *pelB::Psoj (tet)*. The construct was sequenced using oWX507, oWX669, and oWX670.

pWX1093 [*pelB::Psoj-KCK-spo0J(ΔparS)-mgfpmut3 tet*] was constructed by an isothermal assembly reaction containing three fragments: 1) pWX516 digested with HindIII and BamHI, and gel purified; 2) *KCK-spo0J (ΔparS)* amplified from pWX563²³ using oWX2978 and oWX2975; 3) *mgfpmut3* amplified from pWX563²³ using oWX2976 and oWX2977. pWX516 contains *pelB::Psoj (tet)*. The construct was sequenced using oWX507, oWX669, and oWX670.

pWX1103 [*pelB::Psoj-mgfpmut3-spo0J-R80A(ΔparS)-KCK cat*] was constructed by an isothermal assembly reaction containing two PCR products: 1) pWX611 amplified using oWX3001 and oWX418; 2) pWX611 amplified using oWX3002 and oWX2071. This procedure introduced the R80A mutation to pWX611,²³ which is *pelB::Psoj-mgfpmut3-spo0J(ΔparS)-KCK cat*. The construct was sequenced using oWX507, oWX669, and oWX670.

pWX1104 [*pelB::Psoj-spo0J-R80A(ΔparS)-mgfpmut3 tet*] was constructed by an isothermal assembly reaction containing two PCR products: 1) pWX1092 amplified using oWX3001 and oWX418; 2) pWX1092 amplified using oWX3002 and oWX2071. This procedure introduced the R80A mutation to pWX1092. The construct was sequenced using oWX507, oWX669, and oWX670.

pWX1105 [*pelB::Psoj-KCK-spo0J-R80A(ΔparS)-mgfpmut3 tet*] was constructed by an isothermal assembly reaction containing two PCR products: 1.) pWX1093 amplified using oWX3001 and oWX418; 2) pWX1093 amplified using oWX3002 and oWX2071. This procedure introduced the R80A mutation to pWX1093. The construct was sequenced using oWX507, oWX669, and oWX670.

pWX1106 [*pelB::Psoj-soj-spo0J-R80A(ΔparS)-KCK cat*] was constructed by an isothermal assembly reaction containing two PCR products: 1) pWX612 amplified using oWX3001 and oWX418; 2) pWX612 amplified using oWX3002 and oWX2071. This procedure introduced the R80A mutation to pWX612,²³ which is *pelB::Psoj-soj-spo0J(ΔparS)-KCK cat*. The construct was sequenced using oWX507, oWX1086, and oML77.

pWX1107 [*pelB::Psoj-KCK-spo0J(ΔparS) tet*] was constructed by an isothermal assembly reaction containing two PCR products: 1) pWX1093 amplified using oWX3004 and oWX418; 2) pWX1093 amplified using oWX3003 and oWX2071. This procedure introduced a stop codon and removed *mgfpmut3* from pWX1093. The construct was sequenced using oWX507 and oML85.

pWX1108 [*pelB::Psoj-KCK-spo0J-R80A(ΔparS) tet*] was constructed by an isothermal assembly reaction containing two PCR products: 1) pWX1107 amplified using oWX3001 and oWX418; 2) pWX1107 amplified using oWX3002 and oWX2071. This procedure introduced the R80A mutation to pWX1107. The construct was sequenced using oWX507 and oML85.

pWX1167 [*pelB::Psoj-ECE-spo0J(ΔparS) tet*] was constructed by an isothermal assembly reaction containing two PCR products: 1) pWX1107 amplified using oWX3197 and oWX418; 2) pWX1107 amplified using oWX3198 and oWX2071. This procedure introduced the ECE tag and removed the KCK tag from pWX1107. The construct was sequenced using oWX507 and oML85.

pWX1168 [*pelB::Psoj-ECE-spo0J-R80A(ΔparS) tet*] was constructed by an isothermal assembly reaction containing two PCR products: 1) pWX1108 amplified using oWX3197 and oWX418; 2) pWX1108 amplified using oWX3198 and oWX2071. This procedure introduced the ECE tag and removed the KCK tag from pWX1108. The construct was sequenced using oWX507 and oML85.

pWX1169 [*pelB::Psoj-ECE-spo0J(ΔparS)-mgfpmut3 tet*] was constructed by an isothermal assembly reaction containing two PCR products: 1) pWX1093 amplified using oWX3197 and oWX418; 2) pWX1093 amplified using oWX3198 and oWX2071. This procedure introduced the ECE tag and removed the KCK tag from pWX1093. The construct was sequenced using oWX507, oWX669, and oWX670.

pWX1170 [*pelB::Psoj-ECE-spo0J-R80A(ΔparS)-mgfpmut3 tet*] was constructed by an isothermal assembly reaction containing two PCR products: 1) pWX1105 amplified using oWX3197 and oWX418; 2) pWX1105 amplified using oWX3198 and oWX2071. This procedure introduced the ECE tag and removed the KCK tag from pWX1105. The construct was sequenced using oWX507, oWX669, and oWX670.

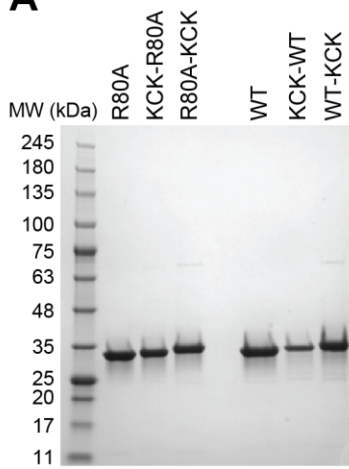
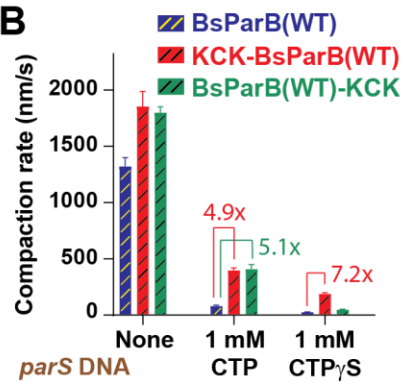
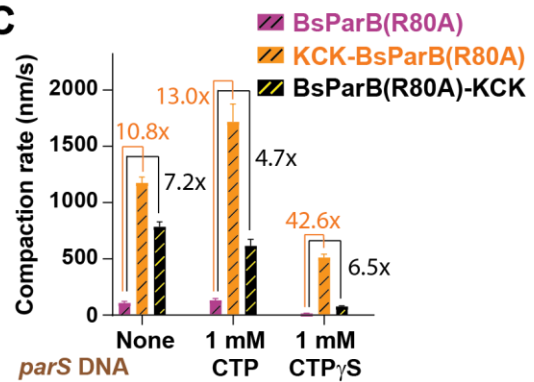
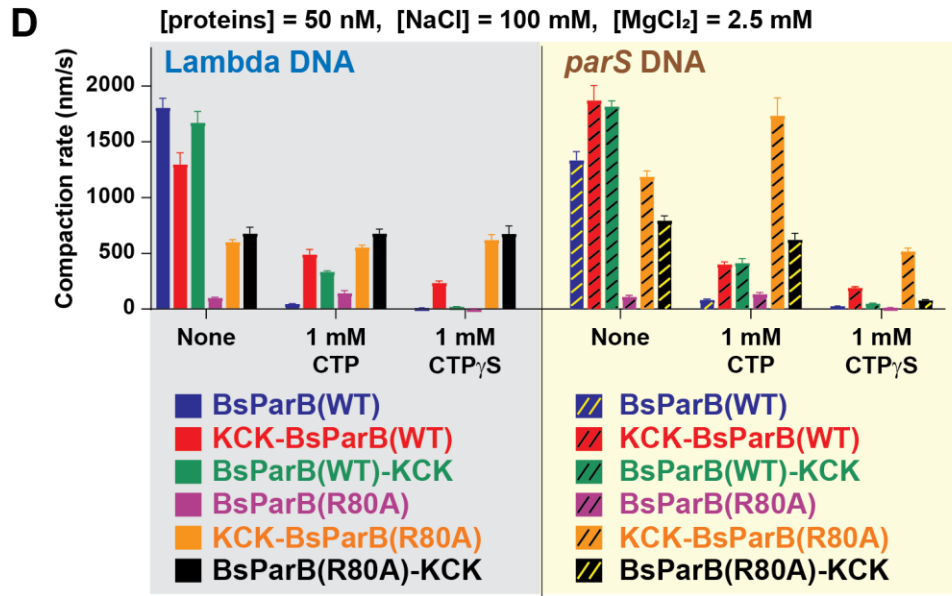
QUANTIFICATION AND STATISTICAL ANALYSIS

Not all measurement groups passed the normality test (See Tab 3 in [Data S1](#)). Therefore, in this study, we report the results of nonparametric Mann-Whitney test in [Figures 1E](#) and [1F](#). However, we obtained similar results from two-sided Welch's t-test ([Figures S5A](#) and [S5B](#)) since the t-test results are still valid when the sample sizes are large (>25) and there are not extreme outliers.⁶⁵ All the statistical analyses (Shapiro-Wilk normality test, Mann-Whitney test, and two-sided Welch's t-test due to different variances and sample sizes) for DNA compaction rates were performed using Prism software (GraphPad, San Diego, CA). The exact sample sizes (n), mean, and standard error of the mean are provided in Tabs 1 and 2 in [Data S1](#). The normality test results are available in Tab 3 in [Data S1](#). Tabs 4 and 5 in [Data S1](#) show the exact p values for comparing wild-type (and its KCK-tagged versions) and R80A mutant (and its KCK-tagged versions) compaction rates, respectively. The reproducibility of single-molecule experiments for each experimental condition was checked by performing the same experiments at least three times.

Supplemental information

**A framework to validate fluorescently labeled
DNA-binding proteins
for single-molecule experiments**

**Miranda Molina, Lindsey E. Way, Zhongqing Ren, Qin Liao, Bianca Guerra, Brandon
Shields, Xindan Wang, and HyeongJun Kim**

A**B****C****D****E**

ns : $p \geq 0.05$ * : $0.01 < p < 0.05$ ** : $0.001 < p < 0.01$ *** : $0.0001 < p < 0.001$ **** : $p < 0.0001$

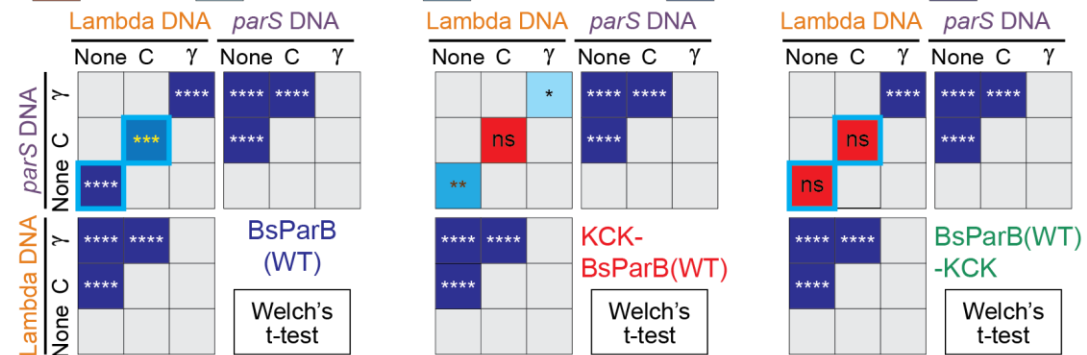
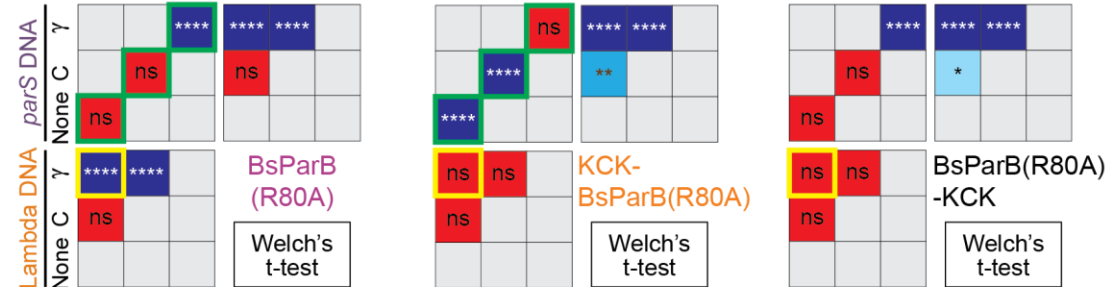
**F**

Figure S1. KCK-tags lead to quantitative and qualitative compaction rate changes, Related to Figures 1, S2, S3, S5, and S7.

(A) InstantBlue Coomassie-stained SDS-PAGE gel of recombinant *B. subtilis* ParB proteins used in this study. The protein ladder (Gold Biotechnology, #P007-500) is on the left. The unnecessary superfluous gel lanes on both sides of this image were removed for clarity.

(B) *parS* DNA compaction rates by BsParB(WT), KCK-BsParB(WT), and BsParB(WT)-KCK proteins in the absence and presence of 1 mM CTP or 1 mM CTP γ S. ($n = 29\sim64$ from 3~5 experiments). Error bars: SEM. The numbers indicate compaction rate fold changes. (C) *parS* DNA compaction rates by BsParB(R80A), KCK-BsParB(R80A), and BsParB(R80A)-KCK proteins in the absence and presence of 1 mM CTP or 1 mM CTP γ S. ($n = 35\sim47$ from 3~4 experiments). Error bars: SEM. The numbers indicate compaction rate fold changes. (D) For direct comparisons, the compaction rates shown in (B), (C) and Figures 1C and 1D are consolidated. ($n = 29\sim74$ from 3~8 experiments). Error bars: SEM. (B-D) See Tab 1 in the Supplemental File S1 for detailed sample number (n) information.

(E-F) Since not all results pass the Shapiro-Wilk normality test, we employed the Mann-Whitney tests to compare DNA compaction rates in Figures 1E and 1F. However, Welch's t-test results are still informative as long as there are not extreme outliers and there are enough (>25) data points [S1]. Indeed, the Welch's t-test results provided here are very similar to the ones from the Mann-Whitney tests. (E) Top: The Welch's t-test p value color scheme. Bottom: The Welch's t-test comparisons for compaction rates by wild-type BsParB and its KCK-versions. (F) The Welch's t-test comparisons for BsParB(R80A) and its KCK-versions. (E-F) Cyan, green and yellow boxes highlight qualitative protein property changes due to the KCK-tags for visual aids. See Tab 1 in the Supplemental File S1 for detailed sample number (n) information.

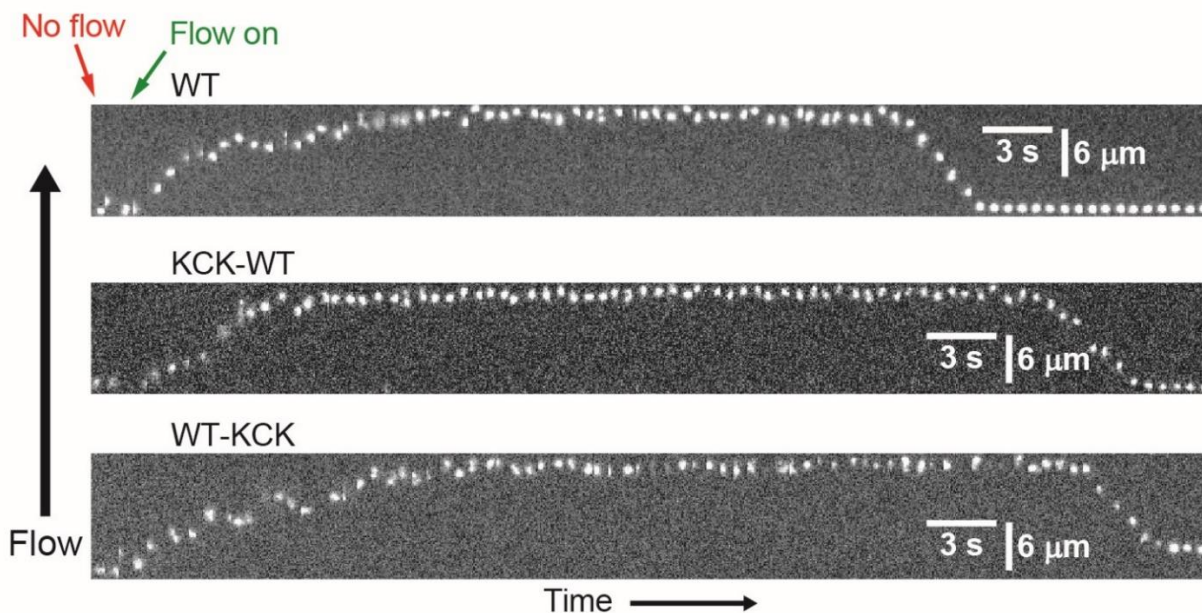


Figure S2. Wild-type BsParB proteins compact DNA towards the tether point, Related to Figures 1 and S1. Representative kymographs for (untagged) wild-type BsParB, KCK-BsParB, and BsParB-KCK proteins. One end of DNA is tethered to the microfluidic sample chamber surface, and the other is labeled with a quantum dot 605. In the beginning, the average quantum dot position is approximately the same as the DNA tether point due to the lack of flow. Turning on the flow stretches DNA. Accompanying proteins lead to the DNA compaction towards the tether point. [Protein] = 50 nM, [CTP] = 0, lambda DNA without any *parS* sites.

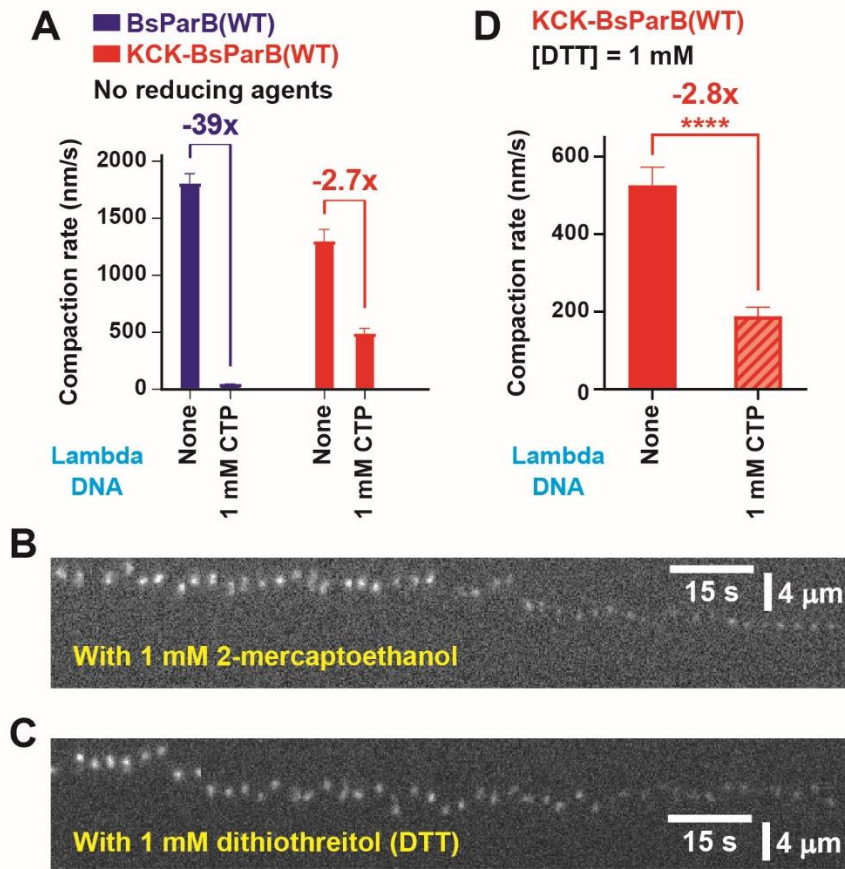


Figure S3. DNA compaction by KCK-BsParB(WT) in the presence of reducing agents, Related to Figures 1 and S1. (A) Lambda DNA compaction rates taken and adapted from Figure 1C for convenient comparison with (D). -39x and -2.7x denote 39-fold and 2.7-fold compaction rate decreases, respectively. (B) A representative kymograph that shows that inclusion of 1 mM β -mercaptoethanol leads to the fluorescence intensity decrease and nonspecific binding of quantum dot-DNA-protein to the flow cell surface. (C) A representative kymograph that exhibits similar technical challenges as (B) in the presence of 1 mM dithiothreitol (DTT). (D) Lambda DNA compaction rates by KCK-BsParB(WT) in the presence of 1 mM DTT both with and without CTP ($n = 39$ from 6 experiments for no CTP and $n = 30$ from 4 experiments for 1 mM CTP). Error bars: SEM; **** $p < 0.0001$. -2.8x denotes 2.8-fold compaction rate decrease.

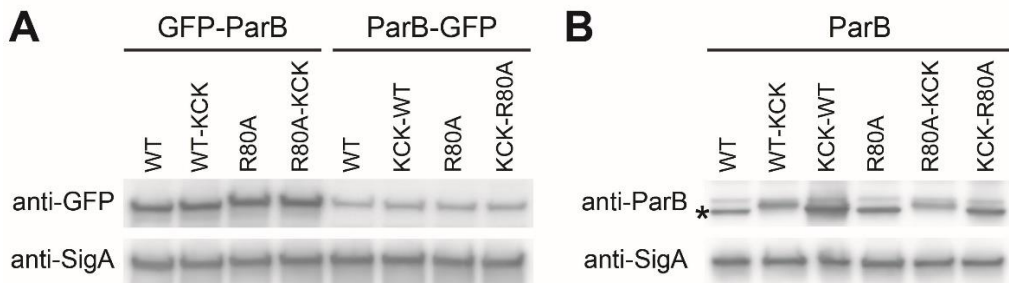


Figure S4. KCK tags do not significantly alter the level of wild-type or R80A ParB, Related to Figure 2. (A) Western blot of GFP-tagged ParB variants. Although GFP-ParB levels are higher than ParB-GFP levels, the R80A mutation or KCK tag does not change the protein levels. SigA levels are shown to control for loading. (B) Western blot of ParB variants. The R80A mutation or KCK tag does not dramatically change the protein levels. Asterisk indicates the ParB band. SigA levels are shown to control for loading. These experiments were performed in two biological replicates and the result from one set of experiment was shown.

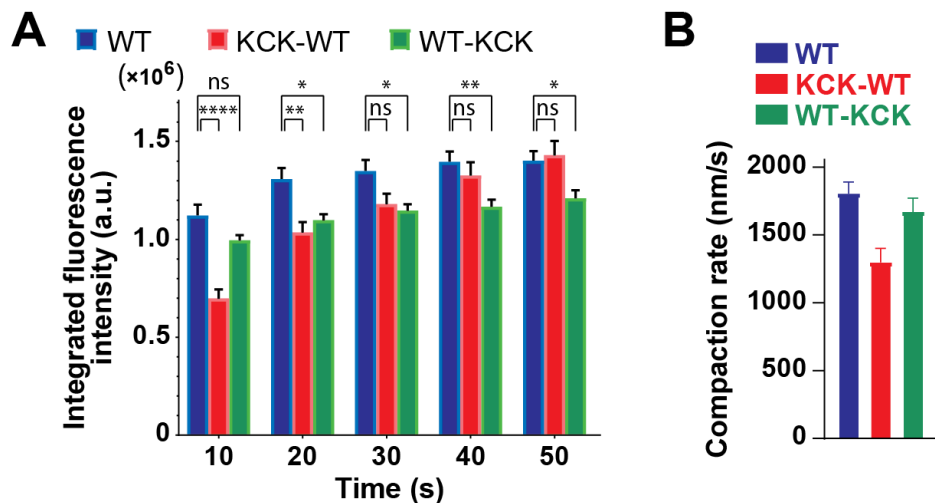


Figure S5. Integrated fluorescence intensities of BsParB(WT), KCK-BsParB(WT), and BsParB(WT)-KCK on lambda DNA, Related to Figures 1, 3, and S1. (A) Integrated fluorescence intensities of BsParB(WT), KCK-BsParB(WT), and BsParB(WT)-KCK on lambda DNA in the absence of CTP ($n = 31\sim47$ from 2~4 experiments). Error bars: SEM; * $0.01 < p < 0.05$, ** $0.001 < p < 0.01$, and *** $p < 0.0001$. (B) DNA compaction rates taken and adapted from Figure 1C for easy comparison with (A).

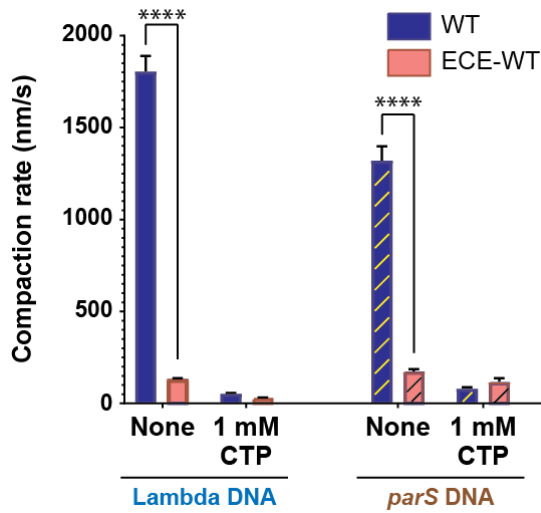


Figure S6. The ECE-tag slows down DNA compaction by the wild-type BsParB protein, Related to Figure 4.
Lambda and *parS* DNA compaction rates by BsParB(WT) ($n = 43\sim74$ from 3~5 experiments), and ECE-BsParB(WT) ($n = 30\sim48$ from 3 experiments) both in the presence and absence of CTP. Error bars: SEM; **** $p < 0.0001$. See Tab 1 in the Supplemental File S1 for detailed sample number (n) information.

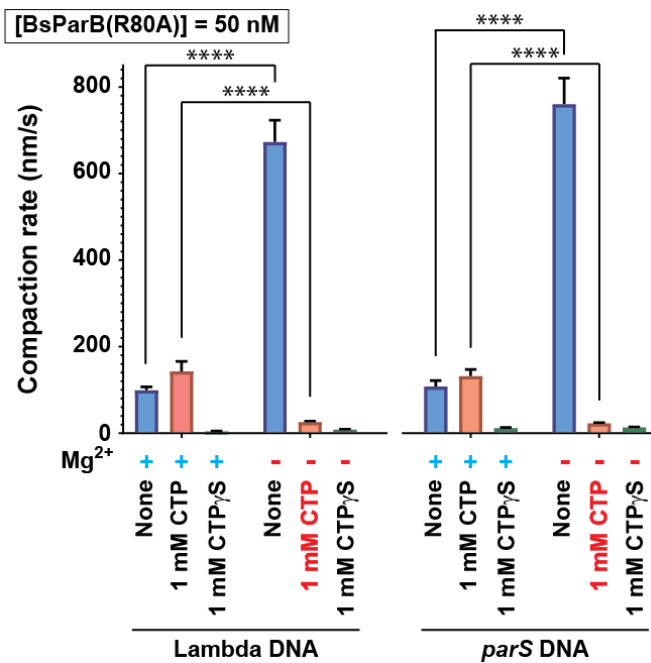


Figure S7. BsParB(R80A) DNA compaction rates in different conditions, Related to Figures 1 and S1.
DNA compaction rates by 50 nM BsParB(R80A) on lambda DNA and *parS* DNA in the presence and absence of magnesium ions ($[MgCl_2] = 2.5$ mM), CTP (1 mM), and CTP γ S (1 mM) ($n = 34\sim58$ from 3~4 experiments). DNA Compaction rates in the presence of CTP and in the absence of magnesium ions are highlighted in red. The absence of magnesium and presence of CTP could explain why the previous study [S2] did not detect DNA compaction by BsParB(R80A). Error bars: SEM; **** $p < 0.0001$. See Tabs 1 and 2 in the Supplemental File S1 for detailed sample number (n) information.

Supplemental references

[S1] le Cessie, S., Goeman, J.J., and Dekkers, O.M. (2020). Who is afraid of non-normal data? Choosing between parametric and non-parametric tests. *Eur J Endocrinol* 182, E1–E3. <https://doi.org/10.1530/EJE-19-0922>.

[S2] Graham, T.G.W., Wang, X., Song, D., Etson, C.M., van Oijen, A.M., Rudner, D.Z., and Loparo, J.J. (2014). ParB spreading requires DNA bridging. *Genes Dev* 28, 1228–1238. <https://doi.org/10.1101/gad.242206.114>.